THE PENNSYLVANIA STATE
UNIVERSITY SCHREYER HONORS
COLLEGE

DEPARTMENT OF MECHANICAL ENGINEERING

Direct Ink Writing of Ethyl Cellulose and Its Composites

TYLER REINERT
SPRING 2023

A thesis
submitted in partial
fulfillment of the
requirements
for a baccalaureate
degree in Mechanical
Engineering
with honors in Mechanical Engineering

Reviewed and approved* by the following:

Amrita Basak
Assistant Professor of Mechanical Engineering
Thesis Co-Supervisor

Zoubeida Ounaies
Professor of Mechanical Engineering
Thesis Co-Supervisor

Amira Meddeb
Associate Research Professor, Materials Research Institute
Thesis Co-Supervisor

Margaret Byron
Assistant Professor of Mechanical Engineering
Honors Adviser

* Electronic approvals are on file.

ABSTRACT

This thesis focuses on the Direct Ink Writing (DIW) of Ethyl Cellulose (EC). EC is a natural biopolymer derived from plants with the capability of revolutionizing the sustainable manufacturing of polymers. Nontoxic, food-grade safe, and insoluble in water, EC is not only sustainable but ideal for pharmaceutical and cosmetic industries. 3D printing is an additive manufacturing technique allowing customization and optimization of small-scale designs at lower costs. Additionally, 3D printing reduces by-products and waste during production, yielding a more sustainable process. In this thesis, DIW is the 3D printing method selected for this thesis due to relative ease of use, access to equipment, and prior success with printing paste-like inks. The printer is developed from customizing a common off the shelf printer. To effectively print higher solid content EC-based inks, the print parameters, such as print speed, gap height, and extrusion amount, must be defined, and their impact on the print must be understood. Furthermore, the composition of the EC ink, including with additives, must be optimized to maximize print quality and curing capabilities. Finally, the curing procedure requires investigation to minimize spreading and maximize solvent elimination, which will maintain print geometry. A series of experiments demonstrated that both the gap height and the print speed have minimal impact on the print within a viable range, whereas extrusion dominates the print geometry. As the solid content of the ink increases, the viable print parameter window shrinks, with only low extrusion yielding predictable results. The addition of silica modified the ink properties, allowing the printability of higher solid content inks with more structural integrity, capable of better maintaining print geometry during curing. Curing at different temperatures and different conditions reveals optimum curing conditions, so the print can be rid of solvent while minimizing spreading. This study of print parameters and curing conditions is necessary to enable the 3D printing of EC inks.

TABLE OF CONTENTS

LIST OF FIGURES

LIST OF TABLES

ACKNOWLEDGEMENTS

I would like to extend my gratitude to Dr. Amrita Basak and Dr. Zoubeida Ounaies for both allowing me to work with them on the project and teaching me how to professionally conduct research in a laboratory setting. Their role as co-supervisors for my thesis research has been a tremendous benefit for completing this project but also providing valuable advice for my professional career. In addition, I want to thank Dr. Amira Meddeb for assistance and advice throughout the project with her expertise in understanding and manipulating material properties. The total support from my advisors on this project has been essential to the completion of my research.

I would also like to take this time to thank Dr. Yuan Xuan. Dr. Xuan put me into contact with Dr. Basak when I was looking to join a laboratory. Dr. Xuan has always been present if I had any questions or concerns. Additionally, Dr. Xuan is an excellent fluids professor, which happened to be one of my favorite classes at Penn State. My current honors advisor is Dr. Margaret Byron who has been eager to answer any questions and help if needed.

This work could not have been completed without the support of the student engagement network (SEN) grant. This program allowed me to pursue the research with more effort and time due to financial and development support.

Finally, I would like to thank my parents Brendan and Betsy Reinert for always pushing me to be my best self, both personally and professionally. Without their support I would not be able to accomplish the things I have done.

Chapter 1

Introduction and Background

Manufacturing is ubiquitous. It is the process of converting raw materials or components into finished products through various techniques such as casting, forging, machining, and assembly. Human ancestors manufactured objects using stone or other tools that date back to at least 2.3 million years ago. The evolution of modern manufacturing can be traced to the industrial revolution when machines were first introduced to replace human labor. Since then, manufacturing has undergone significant changes with the advancement of technology, automation, and globalization. The use of computers, robots, and sensors has made the manufacturing process faster, more efficient, and more precise. In more recent years, there has been an additional focus on sustainability, reducing waste, emissions, and energy consumption. 3D printing of biopolymers has a big role to play in this goal as an alternative for traditional plastics. As well as replacing synthetic plastics, additive manufacturing of biopolymers minimizes production waste, providing a more sustainability manufacturing process. The natural biopolymer of focus for this thesis is Ethyl Cellulose (EC), and the Direct Ink Writing (DIW) printing technique will be used.

1.1 Background

1.1.1 Polymers

Polymers are defined as chains of monomers, ranging from small chains to macromolecules. There are three main classifications of polymers: synthetic, semi-synthetic, and natural [1]. Each type of polymer is used in the manufacturing of materials like rubber, silicone, nylon, plastics, and much more. The use of polymers is essential for numerous industries, due to a large market for plastics, films, and other products derived from synthetic polymers [2].

Synthetic polymers are derived from petroleum in a lab setting and can be classified into four main categories: thermoplastics, thermosets, elastomers, and synthetic fibers. Thermoplastics have had large success in additive manufacturing methods, currently the most common filament used in extrusion-based printing. Examples of thermoplastics include thermoplastic polyurethane (TPU), and Acrylonitrile Butadiene Styrene (ABS) [1].

While all types of synthetic polymers are commonly used, they also share the same challenge related to sustainability. Most synthetic polymers are not biodegradable, so once disposed of, the material may leak toxins into the surrounding environment. Typically, the environment is the ocean, where the toxins impact the water quality and marine life, or landfills, where the toxins can seep into the ground compromising the soil and water sources underneath [1],[2].

1.1.2 Biopolymers

Natural polymers are biodegradable because they are derived from living organisms such as plants. Also known as biopolymers, natural polymers come in many forms, including powder, liquid, or fibers. Due to the large demand for polymers, biopolymers are researched to replace polymer produced products, while improving sustainability. Currently, the only biopolymer produced on a large scale for additive manufacturing is polylactic acid (PLA). Having only one material available limits potential uses, due to limited material properties [1]. By discovering new biopolymer compositions to print, more potential opportunities arise to use a better material. The biopolymer of focus for this thesis is Ethyl Cellulose.

1.1.3 Ethyl Cellulose and its Composites

Ethyl Cellulose (EC) is a naturally occurring biopolymer that can be extracted from wood pulp [3]. Cellulose derivatives were developed and implemented into industry in the early 1900s. Dr. L. Lilienfeld, a practicing medical doctor, discovered Cellulose ether derivatives in 1912, and devoted his research to provide applications in products like rayon and other films [4].

Throughout the course of history, cellulose derivatives have been one of the most common biopolymers implemented across industry [5]. Cellulose biopolymers are inexpensive, abundant, and environmentally safe. Biopolymers also have unique properties that make them attractive candidates in various industries, such as biopharmaceutical, food, cosmetic, and other industries [5]. Ethyl Cellulose (EC) is an inert, nontoxic, insoluble biopolymer that is food grade [3]. Being insoluble while also nontoxic makes EC different from most cellulose derivatives [5]. The polymer

is colorless, odorless, tasteless, and contains no calories. Due to these characteristics, EC has extensive applications in pharmaceuticals, such as release control coating, thin-film coating, and tablet binding [6]. EC is also used as a viscosity modifier and more recently a matrix material in additive manufacturing. [7]. There are many ways to develop EC, particularly printable inks. Ahmadi et al. produced development methods for various uses of EC, discovering that EC was widely compatible and could be additionally joined with other compounds to improve properties, such as electrical conductivity [8].

In most applications, the biopolymer powder must be added to a solvent, which is determined based on application. Common solvents used for EC include alpha terpinol, toluene, butanol, and ethanol [7]. Each cellulose derived material is classified by the cellulose used, the solvent(s) used, and the weight percent of cellulose in the material [9]. The chosen solvent and weight percent relationship determine the fundamental properties of the material, specifically the flexibility and tensile strength. Mechanically, the EC slurry is considered a shear-thinning liquid, meaning it becomes less viscous when forces are applied [3]. Additional inert chemical solutes may be added to impact material properties such as viscosity or density.

The EC chemical composition substitutes some of the hydroxyl groups in cellulose for ethoxy groups, as seen in Figure 1. This substitution forms a basic sugar, making EC a glycoside. Glycosides are organic compounds commonly used in medical applications like heart treatment [6]. Some of the examined properties, such as mechanical strength, stem from the glycosidic bond, which is between the sugar and the new functional group. Glycosidic bonds join monomers in a parallel fashion with hydrogen bonds, yielding high mechanical strength. EC is a semi-crystalline structure, containing some crystalline domains in an amorphous background [3]. Although the

properties vary depending on specific composition, EC has a relatively high melting point, 180 degrees Celsius, and mechanical strength of 45-85 MPa [3]. Due to these desirable properties, EC is considered a quality candidate for additive manufacturing.

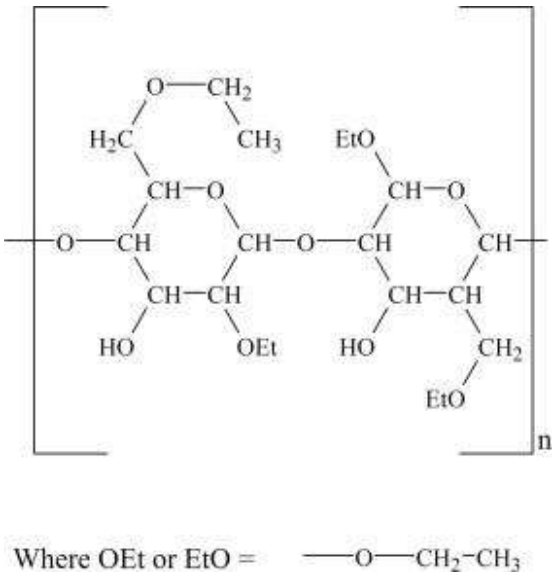

Figure 1:Chemical Structure of Ethyl Cellulose. Figure reference approval from Elsevier [10].

Silica, SiO_2, is a naturally occurring compound that is extremely abundant and can be found in the form of glass, sand, and quartz. Extracted from these natural sources, refined silica is commonly used in industry, due to its well-known and advantageous properties. Additionally, silica has a high melting point and is chemically inert, avoiding any unwanted reaction with materials. Comparatively, silica is also inexpensive for industrial chemical compounds. Silica is primarily used as a thickener, abrasive, and stabilizer. These properties allow silica to prevent separation of mixtures, absorb water to increase viscosity, and provide higher structural integrity and continuity within mixed materials. The abrasive characteristics also provide texture and

cleaning capabilities, such as toothpaste. Silica is only a safety hazard when inhaled if airborne, but otherwise it is commonly used in food and food grade equipment [11].

1.1.4 3D Printing of Biopolymers

Additive manufacturing, or 3D printing, is an industrial process where a design is constructed in layers. Each layer is built upon the prior layer until the final design is completed. 3D printing methods have been around since the late 1980s, but cost-efficient printers were not implemented into the industry until the 2000s [12]. Currently, 3D printers are used to produce complex designs and unique geometries, as well as develop testable prototypes.

Compared to traditional methods, 3D printing provides more design flexibility with limited processing waste during manufacturing [12]. Although many materials can be printed, polymers remain the most common printed material. To improve sustainability, research of biopolymers for additive manufacturing has increased in the past decade. By providing an alternative material with similar characteristics, synthetic polymers could be used less, preserving the environment [9].

The progression of 3D printing has developed numerous printing methods for various materials. Each printing method has unique advantages specific to the material being printed. Biopolymers can print as inks, filaments, and matrix materials [9]. In biopolymer printing the most common printing techniques are selective laser sintering (SLS) and fused deposition modeling (FDM) [13]. SLS is a process where a bed of power is selectively exposed to a high-power laser beam. The beam sinters (fuses) the powdered material, developing a layer of the design. Once a layer is complete, the print area drops a small distance, and a roller pushes a fresh layer of powder

on top of print area. This cyclic process continues until the final design is complete [13]. SLS printers do not require support structures, like other printing methods, and are able to print multiple designs at once. This print method also has high resolution, around 0.08mm [5]. Unfortunately, SLS printers are extremely expensive to purchase and operate. Only around 50% of the powder in the bed can be reused, and the bed must be filled to total print height each time. These prints have low surface finish quality and take an extended time to print and cool [14].

Fina et al. tested manufacturing of both synthetic and biopolymers using SLS for pharmaceutical applications [15]. One of the natural polymers tested was an EC powder. To capitalize on release control capabilities, the research investigated the material and geometry impact to optimize release control accuracy. The geometries printed were bilayer gyroid lattice formations. This is the first investigation of drug release capabilities by a material manufactured by SLS, effectively showing the potential to modify drug release properties through additive processes [15].

FDM is a print method where the filament is extruded through a heated nozzle and deposited on print surface. The filament is fed into the system by rollers, pushing filament out of the nozzle at a specified rate (Figure 2). Upon the completion of a layer, the print surface lowers, or the printhead raises to start the next layer [16]. These printers are cost effective and widely used for simple prototyping and basic designs. Due to relatively thick filament, commonly 1.75mm, the nozzle can only refine the print resolution to around 0.25 mm. This print method also has limited surface finish quality and dimensional accuracy [17].

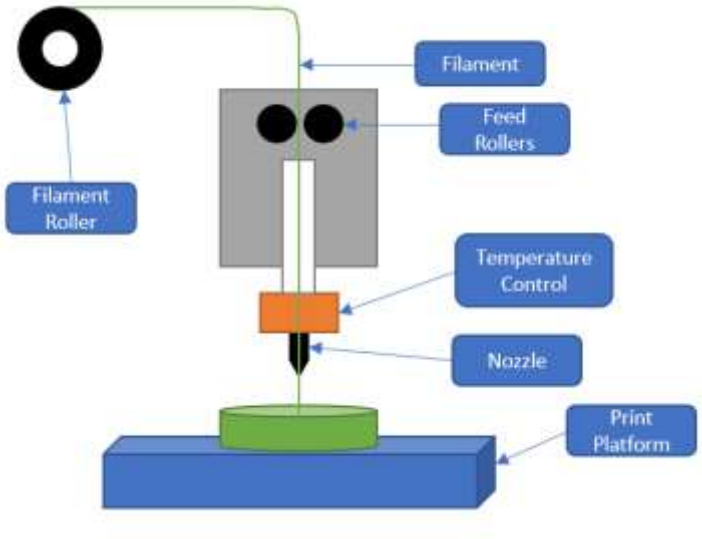

Figure 2: General setup for FMD printing. Figure adapted from Wickramasinghe et al [17].

Regardless of these limitations, FDM remains the most successful print method for EC [5]. In 2018 a team of researchers successfully printed tablets containing EC and ibuprofen, with the intent to print a release-controlled drug. The drug, excipient, and EC were mixed and extruded into filament that could be used for FDM printing. Each tablet extruded measured 4x10 mm, containing internal scaffolding and outer shell. A single layer was 0.2 mm, the shell was 0.4 mm, and the infill density was 25%. Once printed there was further investigation into the release control capabilities and drug density variation of the tablets [18].

Another common biopolymer printed using FDM is Polyhydroxyalkanoate (PHA). Extracted from microorganisms using various exposures of acid, PHA tends to be expensive [1]. To meditate the price, Menčík et al. [19] developed a PHA bio composite to use as filament in FDM printing. They constructed a custom biofilament composite creation device, where composites are created to be printed on a standard FDM printer. This group identified which

filament compositions of PHA yielded the potential to print using FDM. The project was successful, developing multiple filaments capable of printing.

However, the composites lacked the mechanical strength and versatility of commonly printed polymers like PLA [2]. Continuing this line of research, Mencik et al. found that adding a plasticizer would increase the deformation ability by 300% in PHA. The research conducted over the last few years in PHA for additive manufacturing shows the potential to develop new biopolymer composites to use in FDM printing [19].

Along with material limitations, the method of printing also provides limitations. In addition to resolution and other physical constraints (*e.g.*, restricted print size, inefficient for large volumes) each method must be compatible with the given material. For example, FDM printing requires a solid filament that can be melted and rapidly cooled when printed. Each printing method has ideal materials to print, with each material having different advantages [3].

1.1.5 Direct Ink Writing of Ethyl Cellulose and its Composites

Direct ink writing is similar to FDM, except that no heat is applied and the filament is an ink that is extruded through the nozzle. Ink, as opposed to filament, does not need extensive processing and development before printing [20]. The ink, which is commonly a viscous liquid, is extruded at a controlled flow rate through the nozzle [9]. Due to the liquid ink, the sample must be cured post extrusion to solidify. Curing can be accomplished *via* infrared exposure, ultraviolet exposure, or by air drying. Once extruded, the printed ink will spread proportionally to the ink viscosity [16].

Ink can be extruded using pneumatic pressure, a piston, or an augur screw (Figure 3). Each method applies pressure or force on the liquid, extruding a bead through the nozzle. The nozzle for DIW has a finer resolution than FDM, having the capability to print within hundreds of micrometers [20].

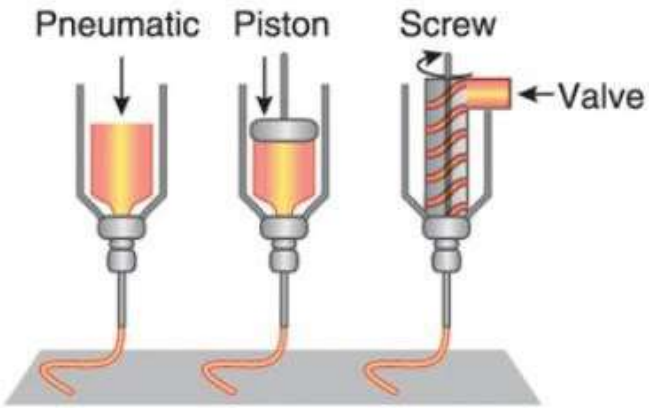

Figure 3: Common methods of DIW. Figure reprinted with permission from [21].

To evaluate the printing quality, three major print parameters are analyzed: print speed, extrusion amount, and nozzle gap height from print surface. By understanding the impact each of these parameters have on the print, printability maps can be created [22]. Each map is dependent on ink type and properties. For example, a higher weight percent ink will have a significantly different map than a lower weight percent ink of the same material [16]. The development of printability maps allows for precision and control when printing. Commonly used materials have been mapped and are well understood [12]. However, most biopolymers have not been mapped or printed using DIW due to the need to cure post printing. Therefore, most commercial DIW printers do not permit the printing of biopolymers due to limited curing capabilities [16].

Recently, researchers at Penn State investigated custom DIW techniques for EC [16], [23]. The studies analyzed the printability of the material extruded from the system and determined the

ideal material and systematic conditions moving forward. Hoopes et al. reviewed the ink development and printing process for ethyl cellulose printed on a custom DIW printer [23]. Each ink had a different weight percent of ethyl cellulose powder. The printer setup had an integrated syringe which functioned as both storage and the nozzle during extrusion. A mounted stepper motor in the printhead drives the syringe down, modeling the piston DIW technique. The physical setup can be seen in Figure 4. With the given physical setup, the amount of extrusion per run is limited to the amount of slurry which can fit into the syringe, approximately 20 milliliters. The goal of the research was to provide proof of concept and material printability for EC on a one-dimensional plane. The testing showed that 10% by weight EC in alpha terpinol yielded ideal printing results, with a uniform bead geometry [23]. The printer design is currently being optimized in the EMC lab at Penn state and can be seen in Figure 4.

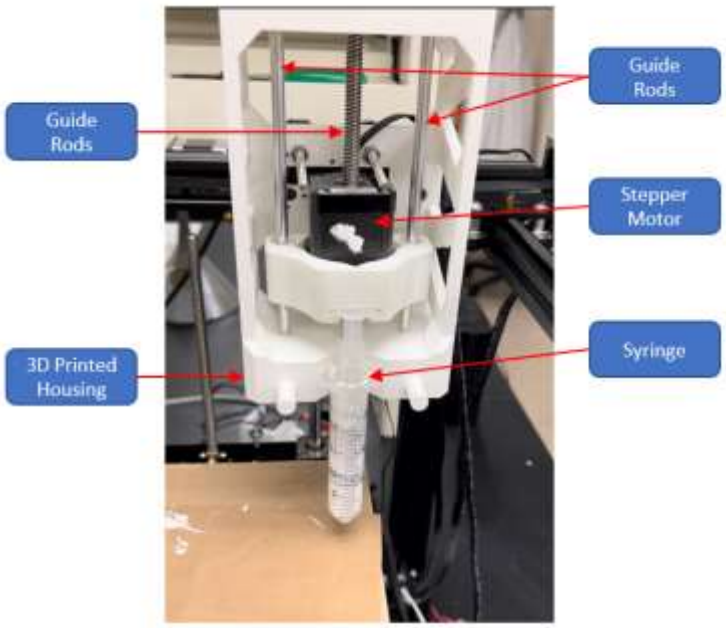

Figure 4: Custom printhead setup for syringe extrusion system. This setup was used to determine printability potential of EC with a piston system.

Adams et al. investigated the following printing parameters: gap height, extrusion rate, and print speed. The custom setup used a 3D printed head with an internal auger screw to push the material out of a nozzle [16]. This setup followed the screw DIW model and can be seen in Figure 5. Like the syringe setup, the screw DIW used an EC powder mixed in an alpha terpinol solvent. This study performed the parameter investigation at 8 weight percent slurry. Experiments tested the impact each parameter had on the printability, which was measured in bead width. The results showed that the extrusion rate was the largest contributing factor to bead thickness, followed by gap height and print speed. The design also provided proof of concept for ethyl cellulose DIW with an auger screw. The research briefly mentioned the curing potential, with an effort to design a curing mechanism within the print space. Overall, curing printed EC has not been explored in quantifiable depth and remains to be investigated [16].

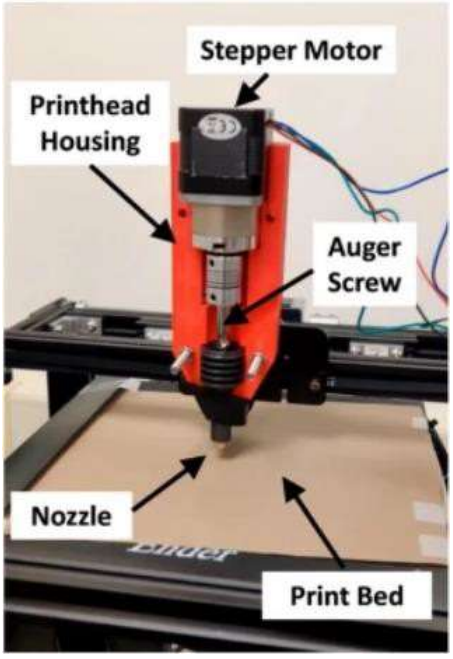

Figure 5: Cross sectional view of DIW screw printer housing. This setup investigated printing parameters. Figure reprinted with permission from [16].

1.2 Problem Statement

Initial DIW of EC has revealed several challenges including spreading of the printed layer, limited curing knowledge, and insufficient layering procedure. The goal of this research is to systematically investigate printing, curing, and layering in an integrated fashion, so the printer may produce functional multi-layer prints of EC at various solid contents. Specifically, the following input parameters are identified: EC ink weight percent, silica weight percent, curing conditions, gap height, print speed, and extrusion. These parameters were varied to assess their impact of the following output parameters, which were considered as indication of successful prints. To accomplish this broad goal, the objectives of the research are:

(1) Understand the impact of solid loading on the printability of multidirectional geometries, such as embedded squares or lines.

(2) Evaluate the effect of adding secondary material such as Silica on the printability.

(3) Understand how available standard curing methods influence material behavior and printability.

Chapter 2

Materials and Methods

2.1 Preparation of EC Ink

First, the solvent α-terpineol [154.25 g/mol with purity of >80% obtained from TCI] is placed in a beaker to be weighed. The EC, [45-55mPa·s, 5% in Toluene + Ethanol (80:20) at 25^{o}C] purchased from TCI, should then be weighed to reach the appropriate weight percent desired and manually mixed. The slurry is prepared and mixed in a heated silicone oil bath, which should reach temperatures of 90 ^{o}C but not exceed 110 ^{o}C. This temperature should be held constant throughout the process using a temperature probe. The beaker is mostly submerged in the hot bath, covered with aluminum foil. Using a magnetic stirrer, the EC is slowly added to the α-terpinol until dissolved. This process of mixing could range from minutes to hours depending on how much solid content is present. Any additional solutes, such as silica, would also be weighed and added in this process. The silica used was purchased from EKI-chem and is pure fumed silica. The magnetic stirrer should be initially set to 60 RPM but increased to 100-200 RPM as viscosity drops due to heat. After the slurry is stirred at temperature for a few hours it can be placed in glass vials, cooled over time, and stored in a cabinet. Depending on the time with magnetic stirrer, degassing upon use may be required. Figure 6 shows the physical setup of the slurry mixing apparatus.

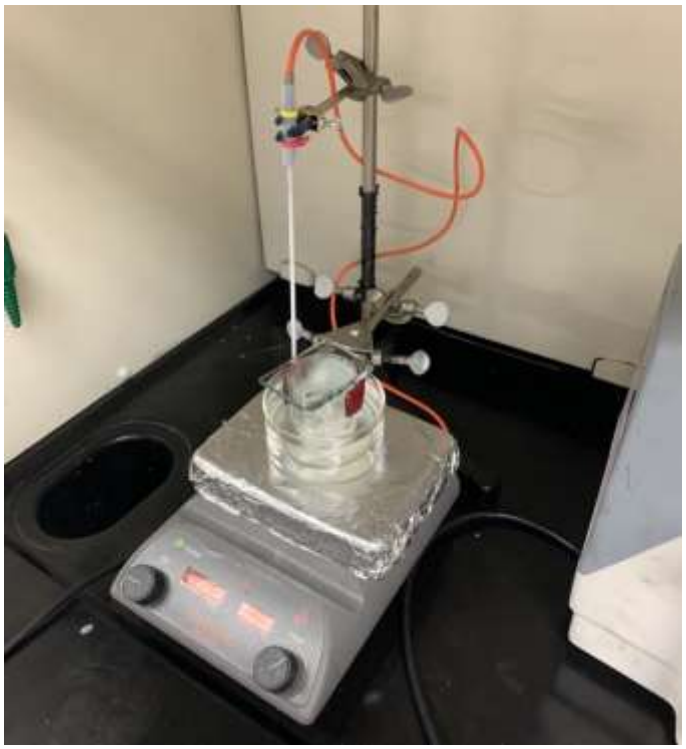

Figure 6: Ink mixing setup with beaker in heated silicon bath.

2.2 DIW Printer Setup

The custom DIW printer is derived from an Ender 5 Pro FDM Plastic Printer from Creality. This printer was chosen due to ease of use and affordability. The Ender 5 Pro has modular features, permitting custom parts to integrate with the system easily. Additionally, the design is fundamental, providing easy access to key circuit connections and sensors. Most of the features and operations remain unchanged except for the printer head, material loading, and extrusion mechanism. The printer functions by executing G-code, which will be discussed in section 2.3.2. The initial development of the printer design is not in the scope of this thesis, but design alterations have been made which will be discussed. The overall printer can be seen in Figure 7.

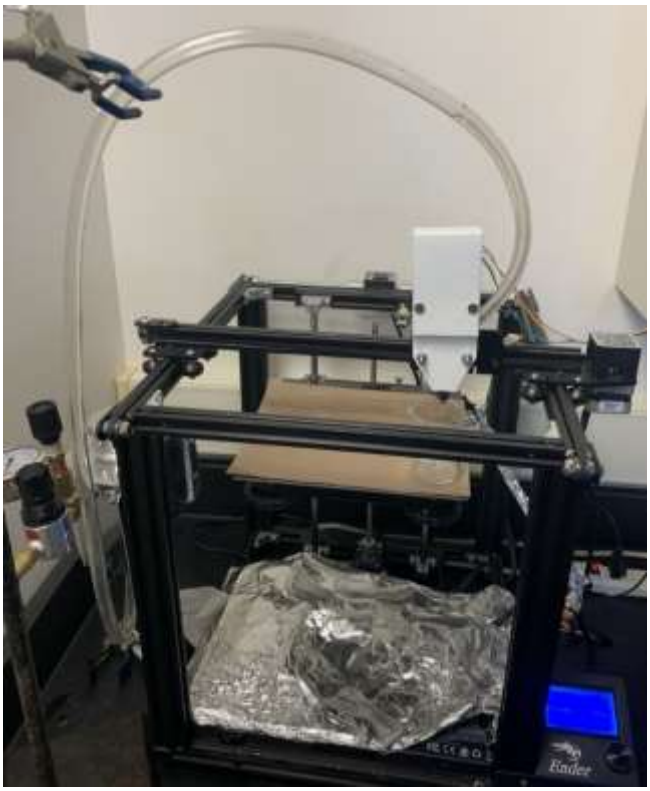

Figure 7:Custom Ender 5 DIW printhead and printer setup.

2.2.1 DIW Printer Setup

The custom DIW printer is adapted from an Ender 5 Pro FDM Plastic Printer from Creality. This printer was chosen due to ease of use and affordability. The Ender 5 Pro has modular features, permitting custom parts to integrate with the system easily. Additionally, the design is fundamental, providing easy access to key circuit connections and sensors. Most of the features and operations remain unchanged except for the printer head, material loading, and extrusion mechanism. The printer functions by executing G-code, which will be discussed in section 2.3.2 Print Parameters. The initial development of the printer design is not in the scope of this thesis,

but design alterations have been made which will be discussed. The overall printer can be seen in Figure 8.

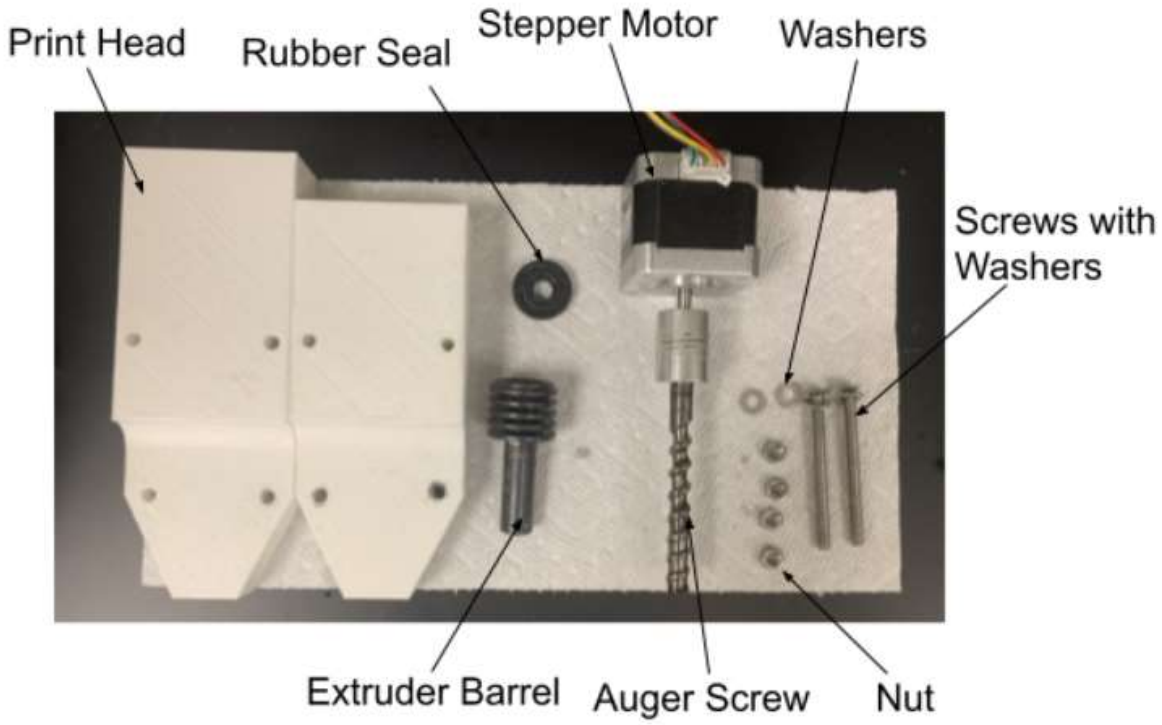

Figure 8: Custom printhead internal components.

The ink is loaded via polyethylene tubing with air pressure, pushing the slurry into the auger screw and extrusion area. The air is not used during extrusion, but only during the loading. While being pushed towards the nozzle, the slurry meets the extrusion barrel. The extruder barrel was chosen for numerous reasons. It was purchased from ROBOTDIG as part number PE-Barrel-D8. The metal part maintains geometry and has a good surface finish, limiting friction between slurry and walls while extruding. A metallic barrel is also easier to clean than an integrated or printed barrel. Finally, the metal nozzle can fit into the extruder barrel with high accuracy to

prevent any leaks during extrusions that require more pressure. The slurry is extruded out of the nozzle in the same fashion as a typical FDM or PLA printer, but without heat.

Throughout the project, the original printhead design has been iterated to improve function. The two main adjustments made to the original design are surface finish and stepper motor casing. To improve cleaning and ink flow for higher viscosity inks, the surface finish was improved by manipulating the print parameters. Using a finer print step in the z direction and thicker shell improved surface finish. Additionally, this change improved the lifetime of the printer. The original design typically lasted around 4-6 months before a replacement was needed. However, with the improved quality the printhead has no signs of needing a replacement, with about 7 months of operation so far. The current printhead can be seen in Figure 9.

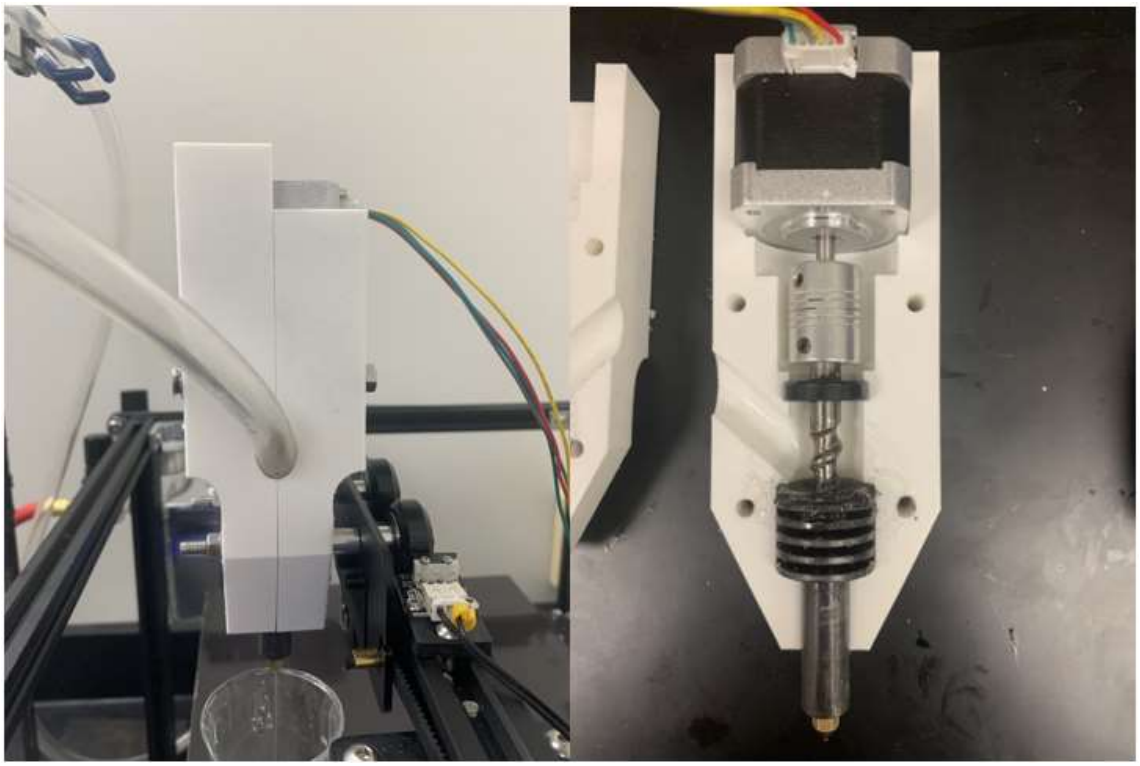

Figure 9: Assembled (left) and cross section (right) of assembled printhead with internal components.

The most important addition to the printhead design was the stepper motor casing. The original design held the stepper motor through a friction fit created when fastening the two printhead halves together. Although this method was sufficient for low to moderate viscosities, when attempting to print high viscosities the friction fit began to fail. The higher viscosity required a significantly larger amount of pressure to properly extrude, which created a force pushing back up on the stepper motor. The force ultimately caused displacement of the stepper motor, which made the printhead ineffective. To prevent stepper motor displacement a simple casing was placed on one half of the printhead shells. This simple rectangular shell constraints the stepper motor in all directions of motion while still providing physical and visual access to the stepper motor components.

2.2.2 Print Parameters

This section discusses the G-code print parameters investigated, print speed, extrusion, and gap height. Every printer has a range of optimal operating conditions that are well established and used during slicing and production of G-code. Since the custom printer has a different print material, loading system, and extrusion method, the G-code parameter functions need to be investigated.

Extrusion amount is a parameter which is represented as E in the G-code. On typical printers this parameter determines how much print material is fed into the printhead and printed. With the custom system the E parameter determines how many rotations the auger screw must

turn, which determines the volume extruded. In section 2.3.3 the exact conversion between magnitude of E and number of revolutions of the auger screw is determined.

Another parameter is print speed, which is not impacted by the custom printhead. However, the print speed, measured in mm/min, needs to be optimized to allow proper bed adhesion and print resolution, as well as being time efficient.

The final parameter investigated is gap height, which is determined by the z axis position displacement from the print surface during extrusion. Gap height also impacts bed adhesion and has a window for good operating. If it is too low, the nozzle will collide with the extruded material, displacing the extruded material to each side of the nozzle. This phenomenon can be seen in Figure 10 and is referred to as tunneling.

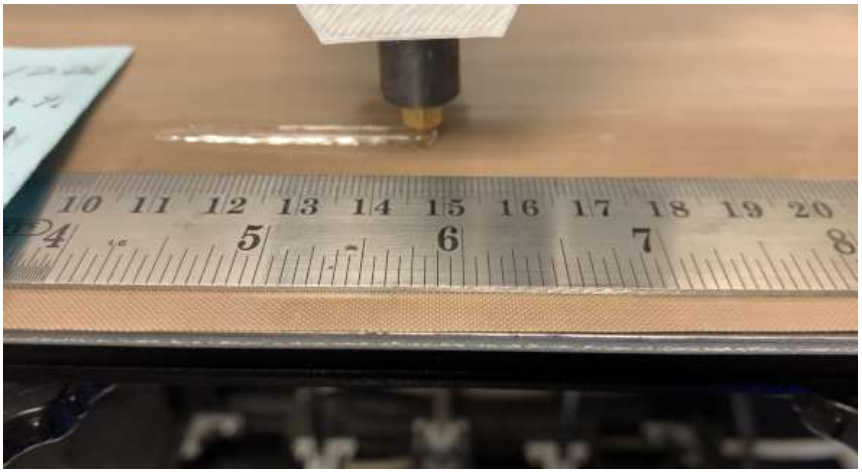

Figure 10: Small gap height causing interference and tunneling with the printed material.

If it is too high, the material may not be able to adhere to the print surface and will simply drag along the print bed. Additionally, the material may buckle or oscillate with a high gap height. This process causes the print to fold over and lay to either side of the print line (Figure 11).

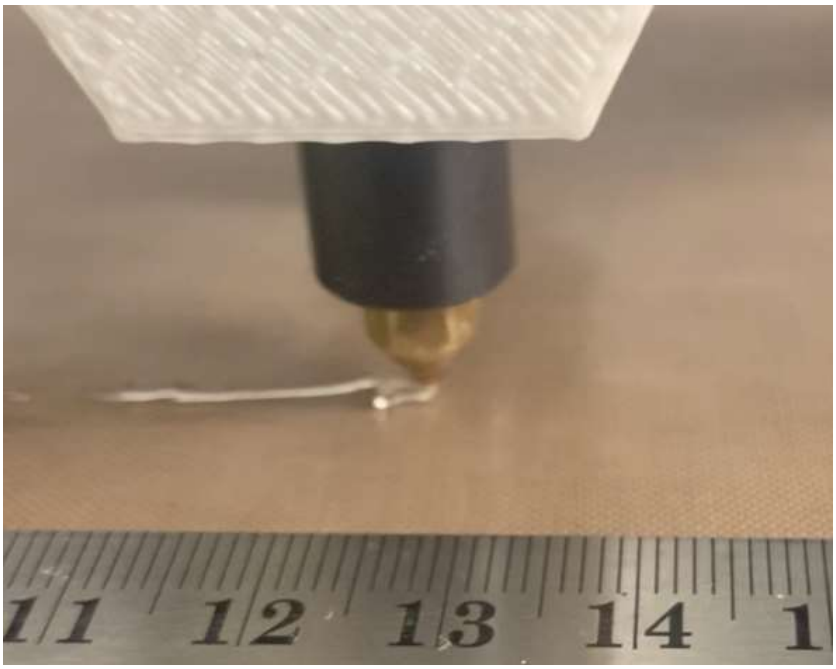

Figure 11: Large gap height causing limited adhesion and buckling.

Each of these parameters are fundamental in creating a quality print. More complex parameters like extrusion rate or total print time are dependent on these three parameters: extrusion value, print speed, and gap height. Therefore, by manipulating the aforementioned parameters the entire print process can be altered.

2.2.3 Extrusion Investigation

During the development of the custom printer the software parameter E was unknown. As discussed in 2.3.2, the E parameter is typically filament length entering extruder mechanism. However, with the change in feed mechanism, the E parameter drove the auger screw, effectively performing the extrusion. It was originally hypothesized that the E parameter represented extrusion rate, due to an increase in extrusion speed when increasing E over the same distance. This

assumption was challenged when more complicated prints with various distances showed variation in extrusion rates with different lengths.

To investigate the true interpretation of the E parameter, a contact tachometer was used to measure RPM of the auger screw when printing different E values at different distances and print speeds. At various print speeds and E values the RPM and total revolutions were recorded and compared. Additionally, the time during printing was recorded and compared to the coded print speed to ensure accuracy in the measurements. This investigation helped to determine parameter independence.

A continuation of this parameter investigation was mass deposition. To ensure independence between the E and print speed parameters, the weight was considered. By printing samples with the same E value and different print speeds, we determined whether print speed impacts mass deposition. E values of 5 and 7 were used for lengths ranging from 75-200mm, as well as speeds ranging from 500-1500 mm/min. This range was selected to verify uniformity in operating speeds of the printability DOE from the work of Adams et al [16].

2.3 Spreading

To successfully print and cure a geometry, the printed material must be able to retain its shape once printed. However, the EC slurry inherently spreads after extrusion, especially when exposed to heat, which is used in the thermal curing process. By determining what loading creates the least amount of spreading, the slurry with most potential for curing and layering was identified.

To test spreading, EC slurries were prepared at 5, 8, 11, 12, and 15 EC weight percent, with the remainder of the weight being the alpha terpineol solvent. Printing parameters were chosen to model the testing previously conducted by Adams et al [16]. Using a 0.6 mm diameter nozzle, a 100 mm line was printed with the maximum values of each parameter: 1mm gap height, 20 mm/s print speed, and 7 extrusion steps. The process was to print a line and measure the spread over time, as quantified by line width. Images including a length scale were taken directly after printing and at set times after printing to a maximum of 15 minutes. Image J software was used to digitally measure the width [24]. Spread measurements were tabulated and organized by slurry composition.

2.3.1 Image J

Image J software was used to extract measurements from digital images taken of experiments. With a known dimension present, used here a ruler, a calibration scale can be established as pixels per mm. For the purpose of this thesis, Image J will be used only for measuring the width of the printed lines. The line tool on Image J is overlaid with the width of the printed line. The software uses the calibration scale to extract the absolute measurement of the line width. This software tool is used for multiple sections of this thesis using the same procedure. An example can be seen in Figure 12.

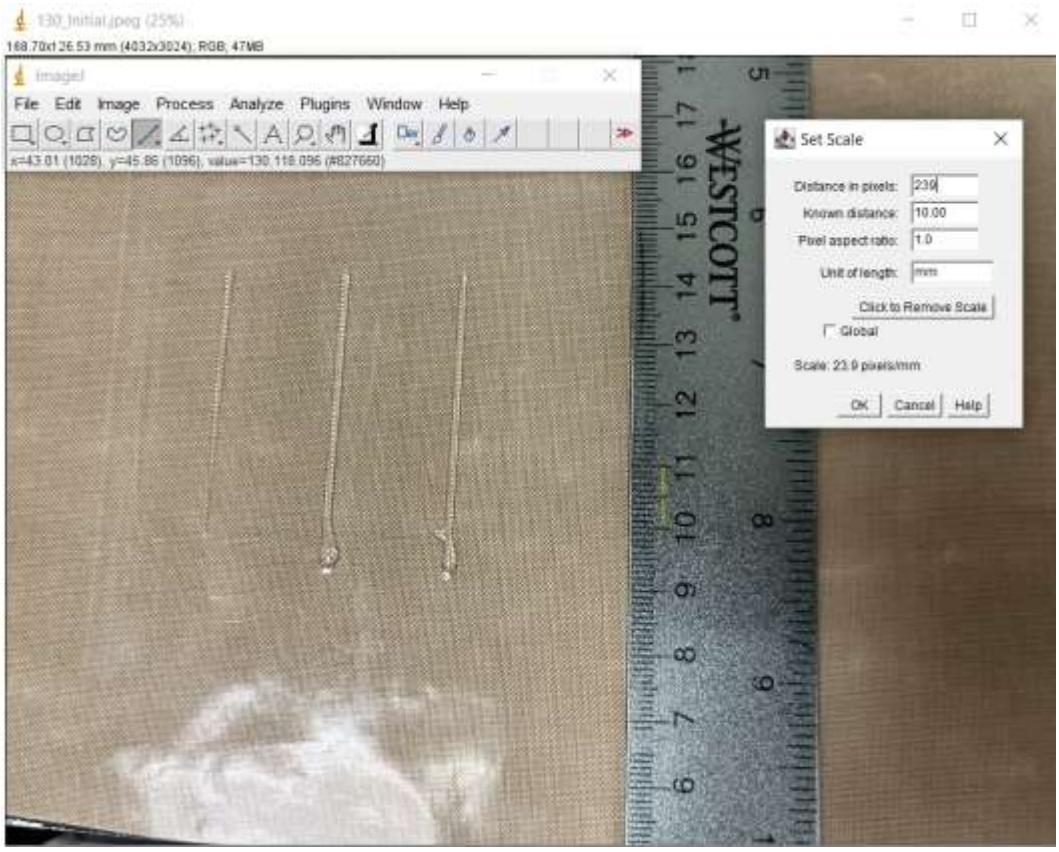

Figure 12: Image J software interface used to digitally measure the width of the lines. The pop-up box shows the pixel scale being set to a known distance, in this case one centimeter.

2.4 Printability Design of Experiment for High Solid Content EC Ink

This section of the thesis describes the design of experiment, DOE, to test printability of high solid content of EC ink. In previous development of the printer Adams et al. developed a printability DOE to determine optimum print parameters for 8 weight percent EC ink [16]. However, to combat spreading upon printing and spreading during curing, a higher weight percent ink is desirable. The higher weight percent composition, the higher the viscosity becomes. Additionally, once the solvent is removed via curing, the print structure will retain more original structures with more solute present. Therefore, a printability investigation for higher EC

compositions is required. Per Adams's trials, three print parameters will be manipulated as three different values. As discussed in section 2.3.2, the print speed, gap height, and extrusion step will be investigated. The three values chosen for each parameter were a minimum, midpoint, and maximum, established by literature and preliminary experimentation at elevated weight percent ink [16]. This method permits interpretation of parameter impact over a large range. To evaluate each combination, 27 trials were conducted as seen in Table 1.

Table 1: Selected parameters to run printability DOE for high solid content EC slurries.

Run #	Print Speed (mm/s)	Gap Height (mm)	Extrusion Step
1	15	1	7
2	15	0.55	7
3	20	0.55	1
4	10	0.1	7
5	10	0.55	1
6	10	0.55	4
7	20	0.1	1
8	10	1	7
9	20	0.55	7
10	15	0.1	7
11	20	1	1
12	10	1	4
13	15	1	4
14	10	0.1	1
15	15	0.55	4
16	20	1	4
17	20	1	7
18	10	0.1	4
19	20	0.55	4
20	10	0.55	7
21	20	0.1	7
22	15	1	1
23	15	0.1	1
24	15	0.1	4
25	15	0.55	1
26	20	0.1	4
27	10	1	1

The nozzle used is 0.6mm diameter. The DOE has two main objectives: collect quantitative dimensions of the print to predict behavior, and qualitatively determine if those print parameters are valid operations for a given slurry composition.

To understand the limitations of the printer, the slurry composition is also manipulated. From preliminary experiments, the printer is unable to print 17 weight percent of pure EC, and from Adams's DOE the highest weight percent composition tested was 11 weight percent. Therefore, the compositions 10, 12, and 15 weight percent were investigated.

2.5 Curing Investigation

Upon achieving printability at high solid contents, the print must be cured for a usable final product. The goal of the curing process is to eliminate most of the solvent, leaving behind a solid bead of solute. The higher the weight percentage before curing, the stronger and more robust the print will be. Due to the high amount of solvent, the cured print loses most of the original print height, typically reducing from 1-3mm to 50-200 microns. Thermal curing is a common method of curing and can be accomplished with various methods. Heating through the bed poses many challenges, with a limited range of temperature and an inability to cure after the first layer is cured. An oven requires too much movement of the print bed, creating alignment issues if printing multiple layers. Therefore, an infrared lamp was used, mounted on top of the printer. For a full description and explanation of the curing setup, see section 2.6.1. However, preliminary testing of pure EC slurries showed ink spread ranging from 200-400 percent, which is unacceptable.

Therefore, there was a demand for ink composition alteration, which would reduce spread without impacting printability.

2.5.1 Curing Apparatus

To cure the print via an IR lamp, the lamp had to be mounted. The IR lamp used had a mounting hole that ran a quarter inch through the back of the lamp towards the handle. Using a quarter inch dowel rod the printer can be suspended by the printer frame using the dowels as support. However, due to the metallic nature of the dowels, conduction through the rods had heat that could damage the printer belts, so the rods could not simply be placed on the printer. To prevent damage to the printer, a simple mounting piece was designed and printed using PLA (see Figure 13 for the final print and Figure 14 for the drawing).

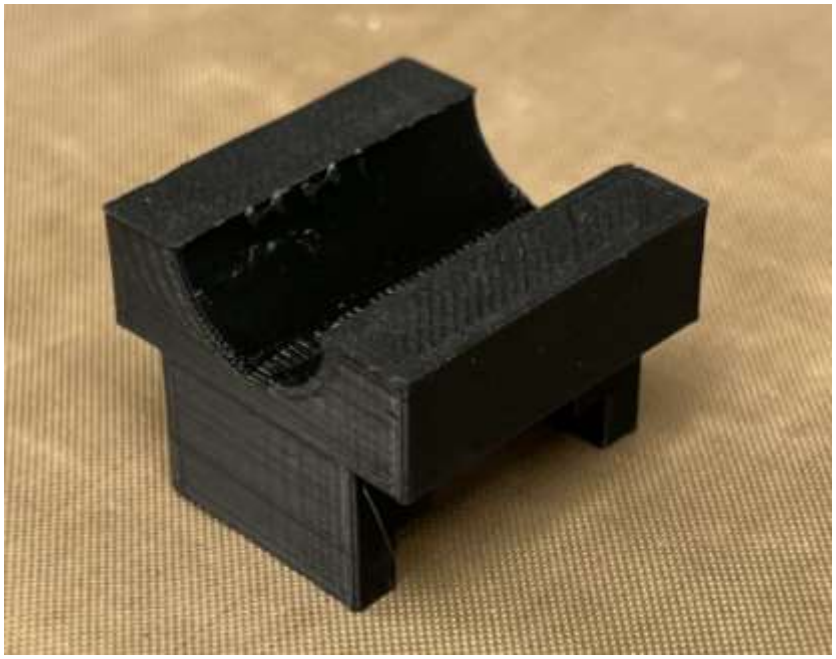

Figure 13: Printed lamp mounting piece.

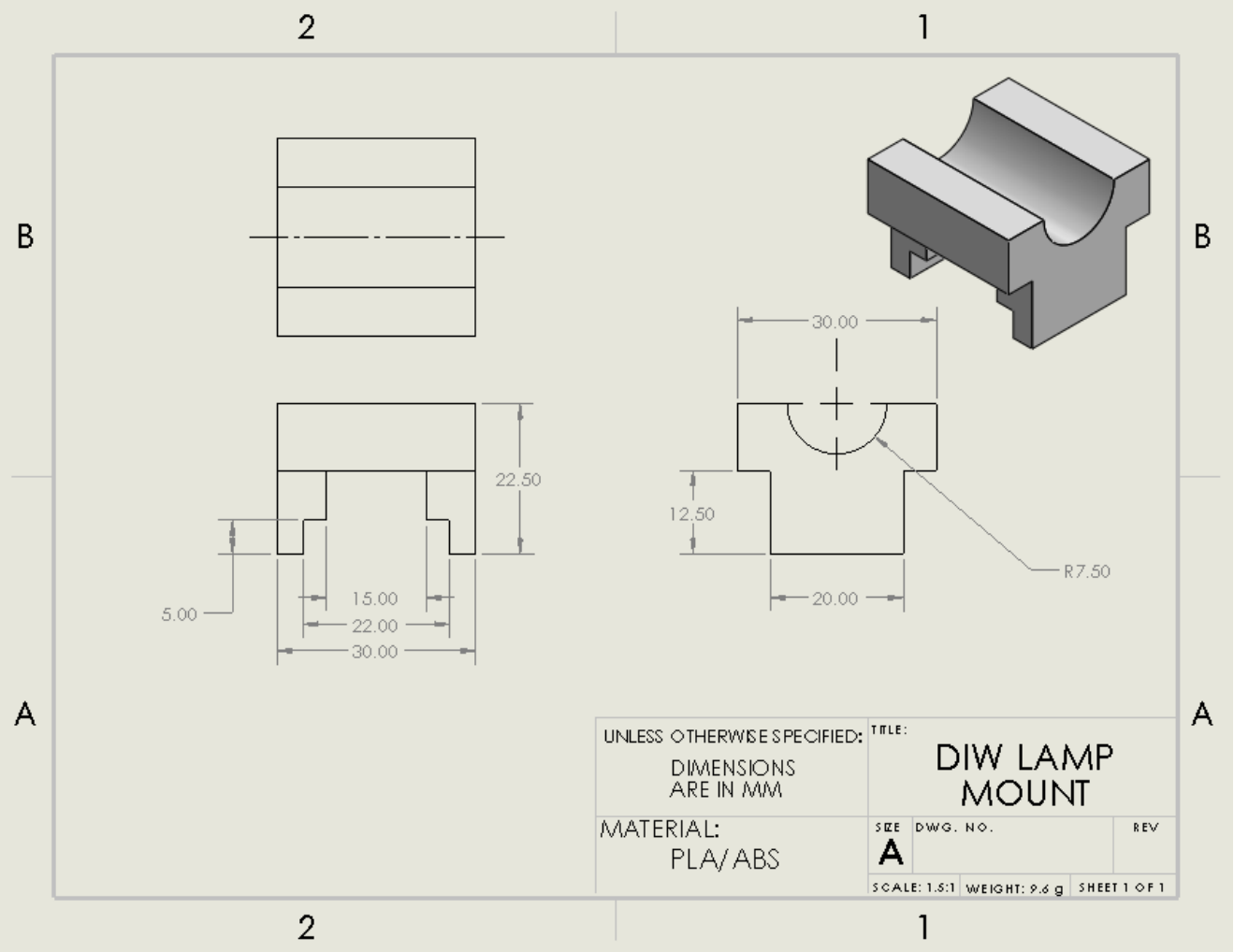

Figure 14: Dimensioned drawing of lamp mounting piece.

This piece holds the rod on one end and fits in with the printer frame on the other. With two mounting pieces, the lamp can be safely suspended above the print bed. The final setup can be seen in Figure 15.

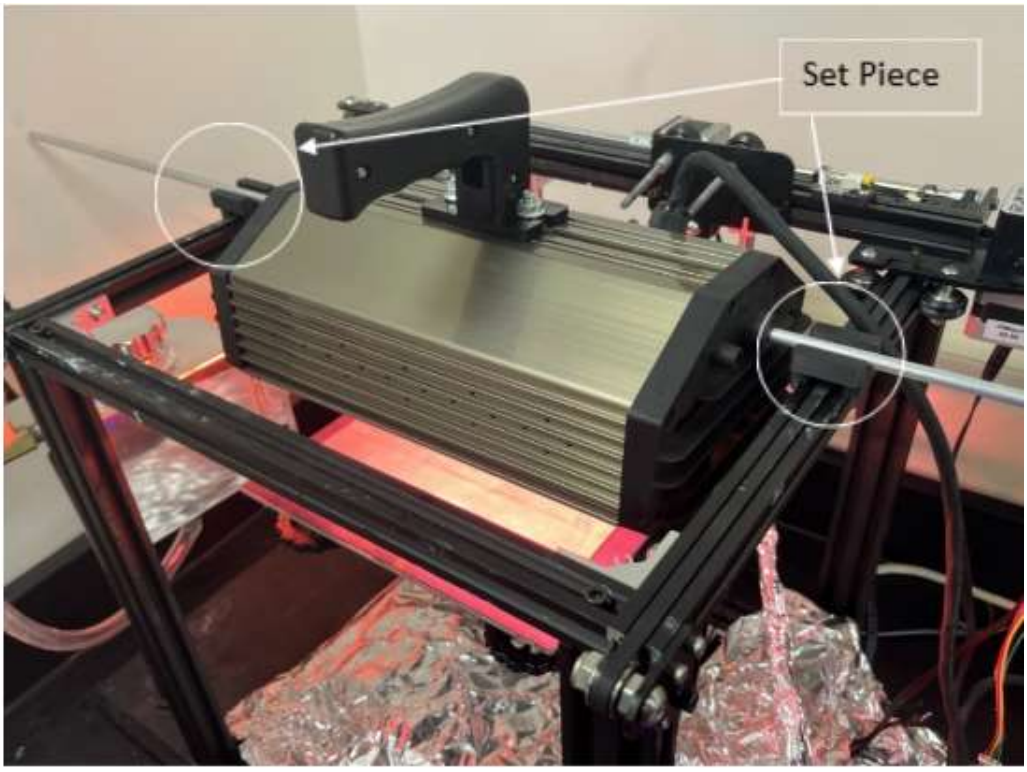

Figure 15: Curing setup with mounted IR lamp on top of printer using the mounting pieces.

It is important to note that the PLA printed material does have a relatively low/average melting point, and the rod becomes hot enough to damage the pieces. Thus far, with over 24 hours of operation, no replacements have been needed, but with higher cure times it is likely this would be a sacrificial piece that would need periodic replacement.

2.5.2 Introduction of Silica

Throughout preliminary curing trials with high weight percent EC, spreading became an extreme issue. Many prints spread 200-400 percent of the thickness once cured when compared to the original geometry. To combat spreading, we aimed to add an inert substance that would add

structure when curing, but not interfere with curing or functionality of the print. Additionally, the added substance needed to allow for printing.

Silica is chemically inert, insoluble in water, relatively inexpensive, and readily available. Upon the addition of silica in small quantities, we observed the emergence of a unique property. Previous EC inks were very viscous and adhesive, whereas inks with silica present became more cohesive. The slurry could be rolled as opposed to smeared and holds shape. This fundamental change in the slurry property changes the ability to extrude. With high weight percent EC, the slurry stuck to the side walls and auger screw, clogging the system and preventing proper extrusion. With the silica added to the slurry, the property change allows high solid content slurries to be printed. Additionally, the increase in viscosity and cohesion prevents spreading post print. An example image of the internal integrity of printed slurry can be seen in Figure 16.

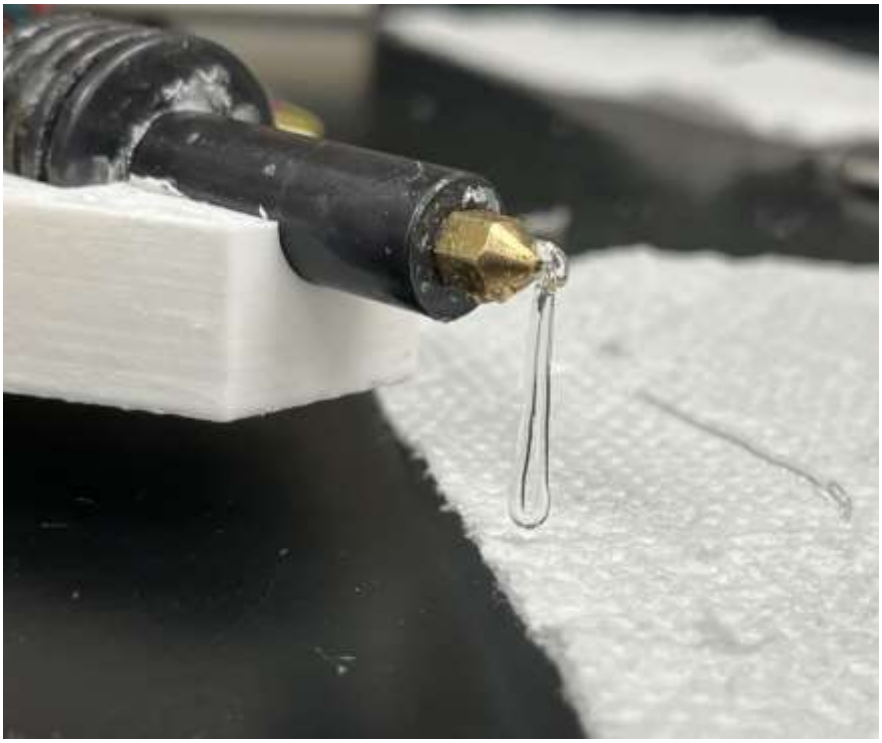

Figure 16: EC and slurry loaded with Silica maintaining structure despite hanging with no support.

To optimize curing, both the curing temperature and slurry composition were investigated via a DOE. From preliminary testing, three temperatures and three compositions were selected from the viable ranges. Following the procedure outlined in section 2.5, three lines were printed. The printing parameters were held constant with print speed at 2000 mm/min, gap height at 1 mm, and E step at 1 per 50 mm. Once printed an image is taken of the print with a scale present and a timer is started. By probing with a spatula and observing, the sample is deemed cured when it becomes rigid, and no more solvent can be observed burning off. After curing, a final image is taken from the same position with the same scale. The samples are taken off the print plate, labeled, and stored for later sample analysis.

2.5.3 Differential Scaling Analysis

Differential Scanning Calorimetry, or DSC, is a thermoanalytical technique measuring the difference in the heat required to change the temperature of a sample to a known reference. Using this analysis technique can yield the glass transition temperature, T_g., which is the temperature at which the amorphous region of the polymer transitions from a glassy/rigid state to a rubbery/soft state [25]. This value, when compared relative to each other, can lead to conclusions about the effectiveness of the curing in the sample [26]. Additionally, the glass transition temperature can provide insight into stability and durability of the material. Polymers with high T_g tend to be more rigid and have higher operation temperatures. Low T_g polymers tend to soften and deform at high temperatures.

To prepare a sample for the TA Instruments DSC, the sample was first sliced into 4 mg segments and loaded into a Tzero Aluminum pan. The pan was sealed with a cap via a press and loaded into the machine at a known position. The sample weight and position number were recorded. The DSC test runs in two heating/cooling cycles at a set ramp rate. Referencing literature about pure EC testing, the range of 40-250 degrees C with a ramp rate of 20 degrees per minute was selected [27]. Two cycles were performed, where the first cycle represents the initial sample behavior with its thermal history. The second cycle represents the sample's thermal behavior without an input from its thermal history. Once both cycles are completed the data can be observed through TA Universal Instruments (Figure 17).

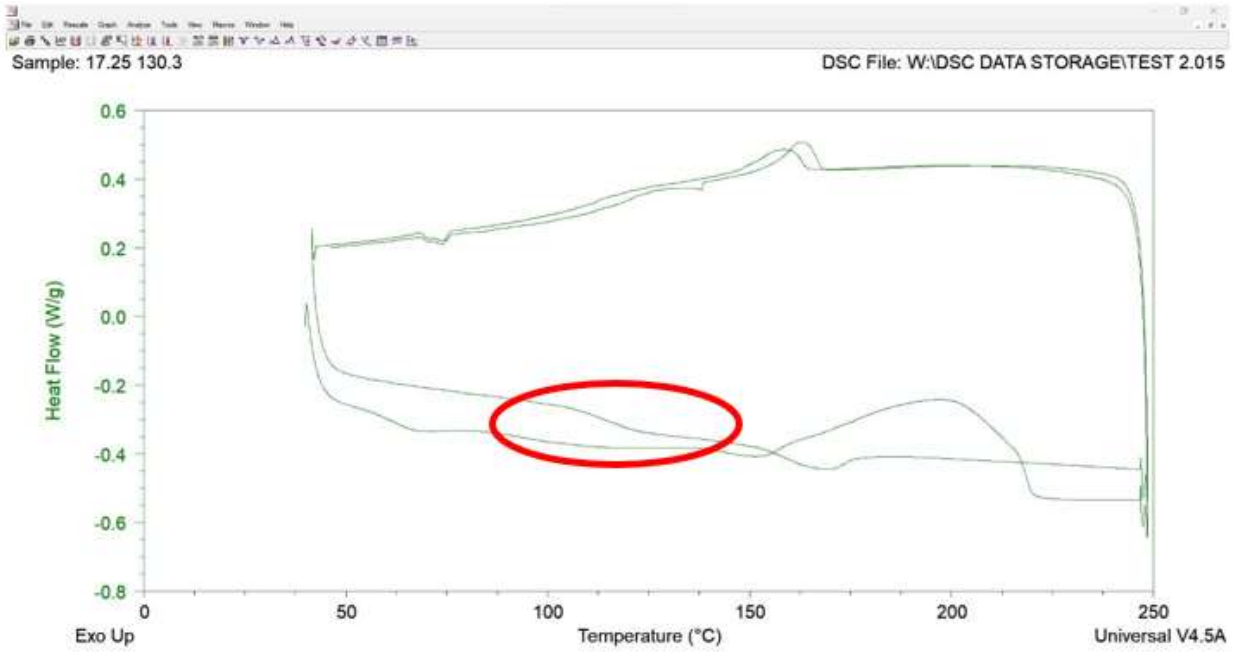

Figure 17:2 Cycles of DSC process plotted.

To ascertain the T_g of the sample the second cycle was observed. The T_g is the midpoint of the inflection point during the heating process (red outlined area, Figure 17). TA Universal Instruments has a tool to assist in finding T_g, where the beginning and ending of the inflection are

selected, and the midpoint is calculated. An example of the T_g fitting can be seen in Figure 18. The T_g is designated with the (I) following the temperature reading, while the other temperatures represent the bounds which were manually selected.

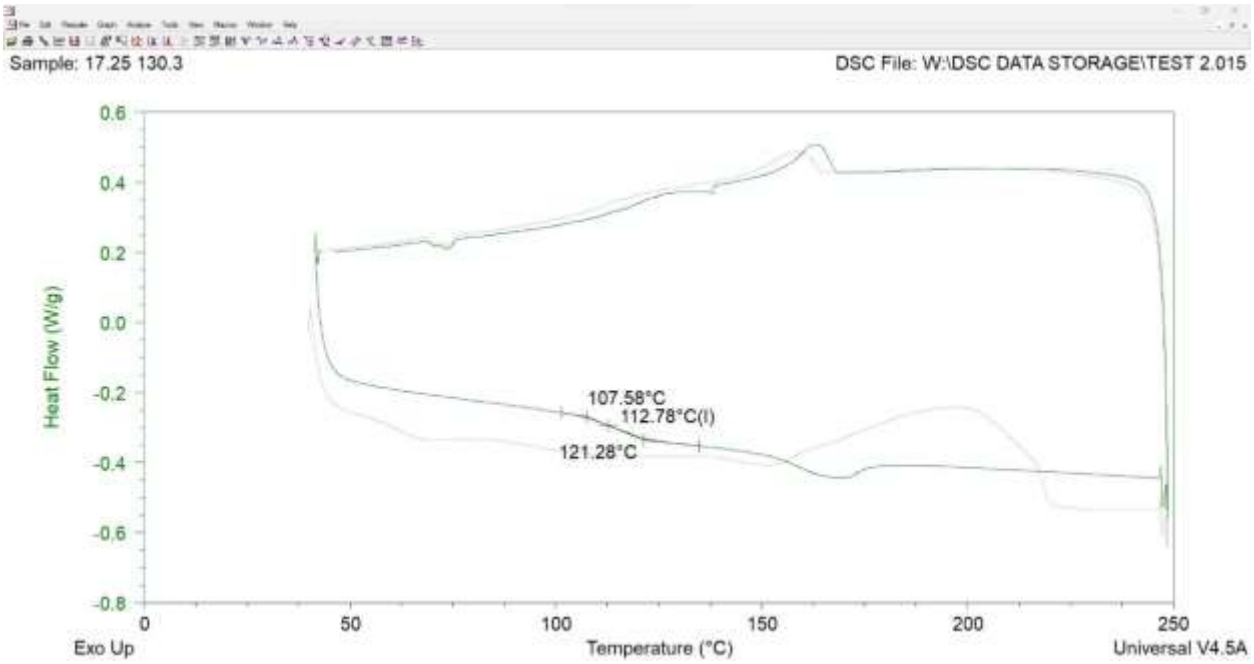

Figure 18: Tool to extract T_g from DSC second heat curve.

Chapter 3

Results

3.1 Impact of EC Loading on Printability

To fully understand the impact of EC loading on printability and potential print application, an investigation into the fundamental print outcomes was undertaken. Due to the ink viscosity, once printed the EC will spread. Additionally, the custom printhead setup created an unknown impact on parameter independence.

3.1.1 Spreading

To understand the limitations and behavior of spreading, line width was recorded over a 15-minute timeframe post print using digital measuring via ImageJ. Figure 19 displays the line width measured over the allotted timeframe for 5, 8, 11, 12, and 15 weight percent EC slurries. Additionally, Figure 20 shows the width rate of change between each time interval.

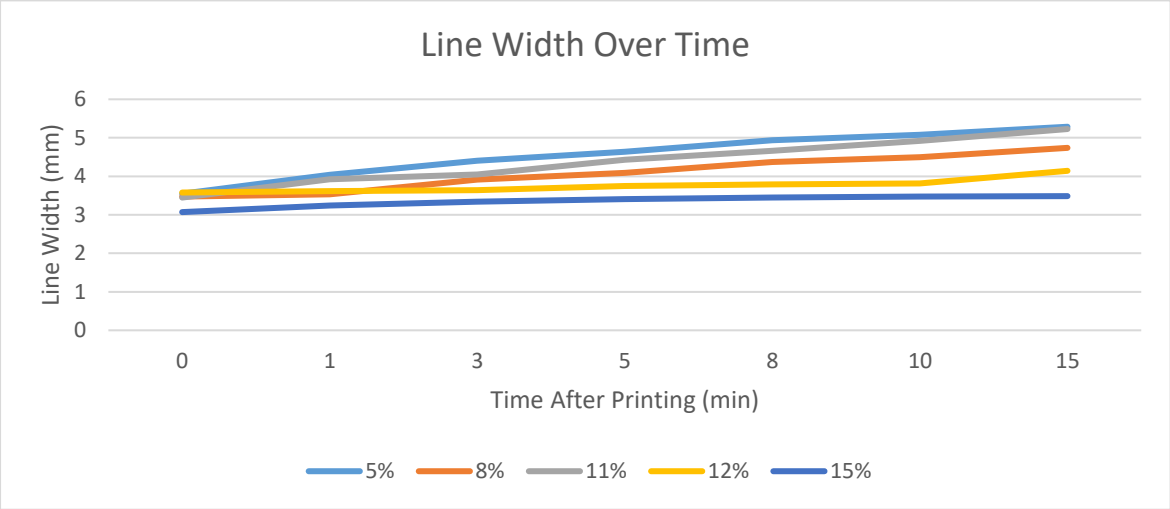

Figure 19: Pure EC spread over time post print.

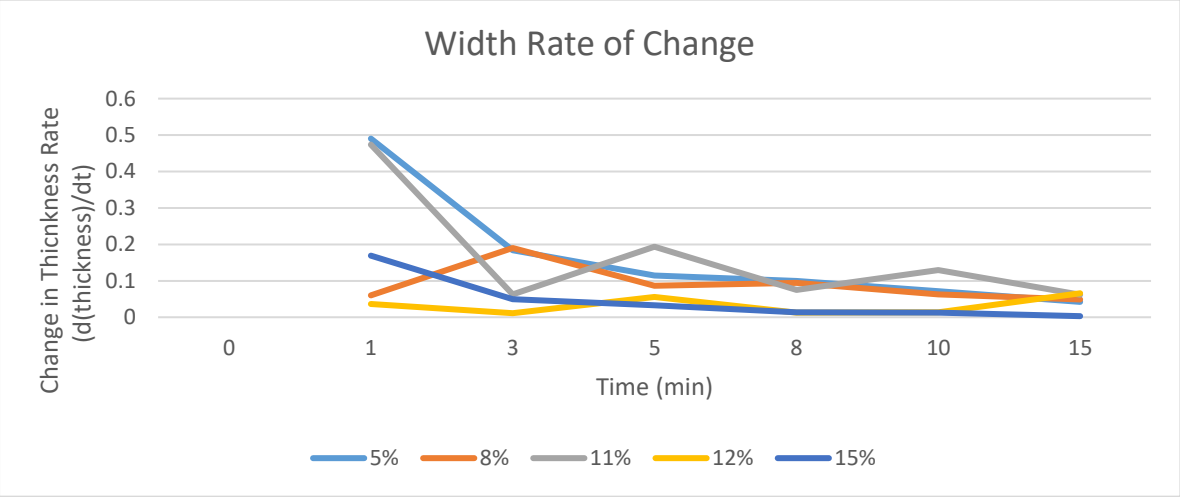

Figure 20: Pure EC spread rate over time post print.

As expected, we see an inverse relationship between solute content and spreading. This relationship stems from the discrepancy in viscosity. The larger amount of solute creates a more viscous slurry, yielding a higher resistance to spreading. Ideally the post print spread should be minimized to permit prints with higher accuracy and resolution. This basic understanding of post print behavior provides the driving motivation to achieve printability at higher weight percents of

EC. Additionally observed is a slight dip in initial line width from 12 to 15 weight percent. This disparity aligns with preliminary testing of higher weight percents, showing lower line widths printed with the same print command. With a custom printhead this observation revealed the need to verify and understand the G-code parameters and parameter independence.

3.1.2 Parameter Independence

Due to the DIW auger screw method of application, as opposed to traditional filament extrusion, the parameter independence and interpretation of G-code parameters was unknown. The E step, typically in control of feed rate, was speculated to be the extrusion rate or extrusion amount. Using a tachometer and stopwatch, we measured print time and auger screw revolutions (Table 2).

Table 2: E parameter investigation.

Extrusion Value	Print Speed [mm/min]	Distance [mm]	Measured RPM	Measured Run Time [sec]	Print Speed Calculation Check [mm/min]	Total Revolutions	Revolutions per Extrusion Value	Extrusion Rate [revs/sec]
2	600	100	22	10	600	**3.67**	1.833	0.367
2	900	100	33	6.69	897	**3.65**	1.823	0.545
2	1200	100	44	5	1200	**3.63**	1.813	0.725
3	600	100	32	10	600	**5.40**	1.800	0.540
3	900	100	49	6.69	897	**5.45**	1.817	0.815
3	1200	100	65	5	1200	**5.40**	1.800	1.080
4	600	100	44	10	600	**7.25**	1.813	0.725
4	900	100	65	6.69	897	**7.29**	1.823	1.090
4	1200	100	87	5	1200	**7.23**	1.808	1.447
5	600	100	54	10	600	**9.03**	1.807	0.903
5	900	100	82	6.69	897	**9.14**	1.829	1.367
5	1200	100	108	5	1200	**9.03**	1.805	1.805
6	600	100	65	10	600	**10.83**	1.806	1.083
6	900	100	98	6.69	897	**10.93**	1.821	1.633
6	1200	100	130	5	1200	**10.83**	1.806	2.167
7	600	100	76	10	600	**12.70**	1.814	1.270
7	900	100	115	6.69	897	**12.77**	1.824	1.908
7	1200	100	152	5	1200	**12.64**	1.806	2.528
Distance Check								
7	1200	200	76.2	10	1200	**12.7**	1.814	1.270
7	1200	75	215	3.54	1271	**12.685**	1.812	3.583

Despite changes in print speed and distance, the number of revolutions remains the same for a tested extrusion value (bolded in Table 2). Therefore, the E step does not represent a rate, but instead number of revolutions of the stepper motor. Using the measured revolutions and the extrusion value, the number of revolutions for each unit of E was established at around 1.81 revolutions.

With this understanding of the extrusion value, conflicting preexisting assumptions were challenged. Throughout testing prior to extrusion value investigation, there was a notion that the mass deposited was dependent on the print speed. However, it has been proven that the print speed

and number of revolutions are independent of each other. Regardless of speed or distance, an extrusion value sets the number of stepper motor revolutions for that line. At higher print speeds the stepper motor is required to revolve at a higher speed, but the total number of revolutions stays the same (and vice versa for lower speeds). Therefore, a variance in mass deposition at different speeds would be unintuitive, unless there is a nonlinear relationship between extrusion flow and revolution speed. Due to the slurry composition the printed material acts as a shear-thinning liquid. Although it is likely this relationship is complex and nonlinear over its entirety, we can approximate the relationship is linear in a smaller operating range. This hypothesis stems from deposition variation only being observed when comparing extreme cases. Traditional printers use various print speeds to allow designer manipulation of the quality-time trade off. Using a limited range hinders the ability to control this relationship but allows for predictable and consistent mass deposition. To test, lines were weighed when printed at 5 speeds, as well as two extrusion values (Figure 21).

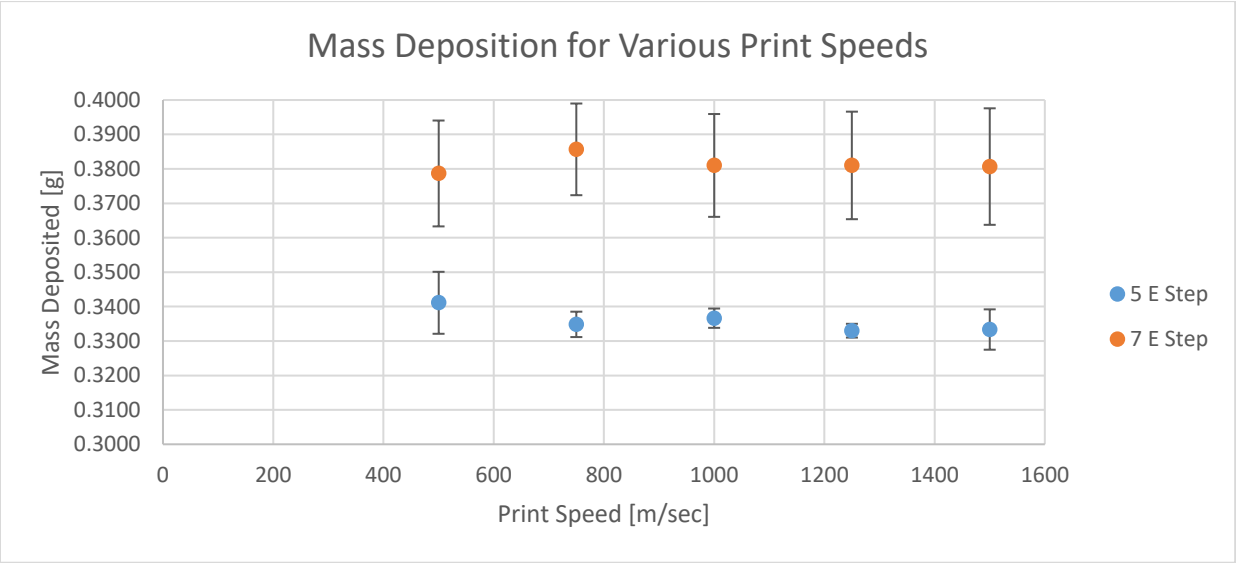

Figure 21: Mass deposition check at various print speeds during printing. This data verifies the parameter independence conclusion.

For both cases, the print speeds created no apparent difference in the mass deposited. This testing verifies that with a limited print speed operation window, the print can be assumed to have equivalent total deposition. Tested here are speeds from 500-1500 mm/min in 250 mm/min increments.

Through parameter testing and mass deposition investigation, the G-code parameters are proven to be independent within a selected range. Understanding this independence allows conclusions to be drawn about the printability of the material, as opposed to issues with parameter operation. This process also established known associations with each parameter that were previously arbitrary.

3.1.3 Design of Experiment

This section of the thesis describes the results from the printability DOE for increasing weight percents of pure EC. Tested are 10, 12, and 15 weight percent EC with variation in testing parameters of extrusion, gap height, and print speed. The parameter ranges were selected to model the DOE previously performed by Adams, who used lower weight percentages of EC [16]. To quantify the impact each parameter has on the print, ImageJ was used to digitally measure the line width.

From the parameter independence defined by the extrusion rate investigation, changes in gap height and print speed should have little to no effect on the print width. However, within these operation ranges, combinations could result in failed or misconstrued widths. With low gap heights and over extrusion, interference with the nozzle and printed material can lead to exaggerated print

widths. Additionally, if the gap height is too large, material can drag, curl, and buckle before meeting the print surface. Prints experiencing these errors were reprinted and not included if issues continued. Figure 22 shows the prints widths for each run of the 10 weight percent EC printed with the varied parameters.

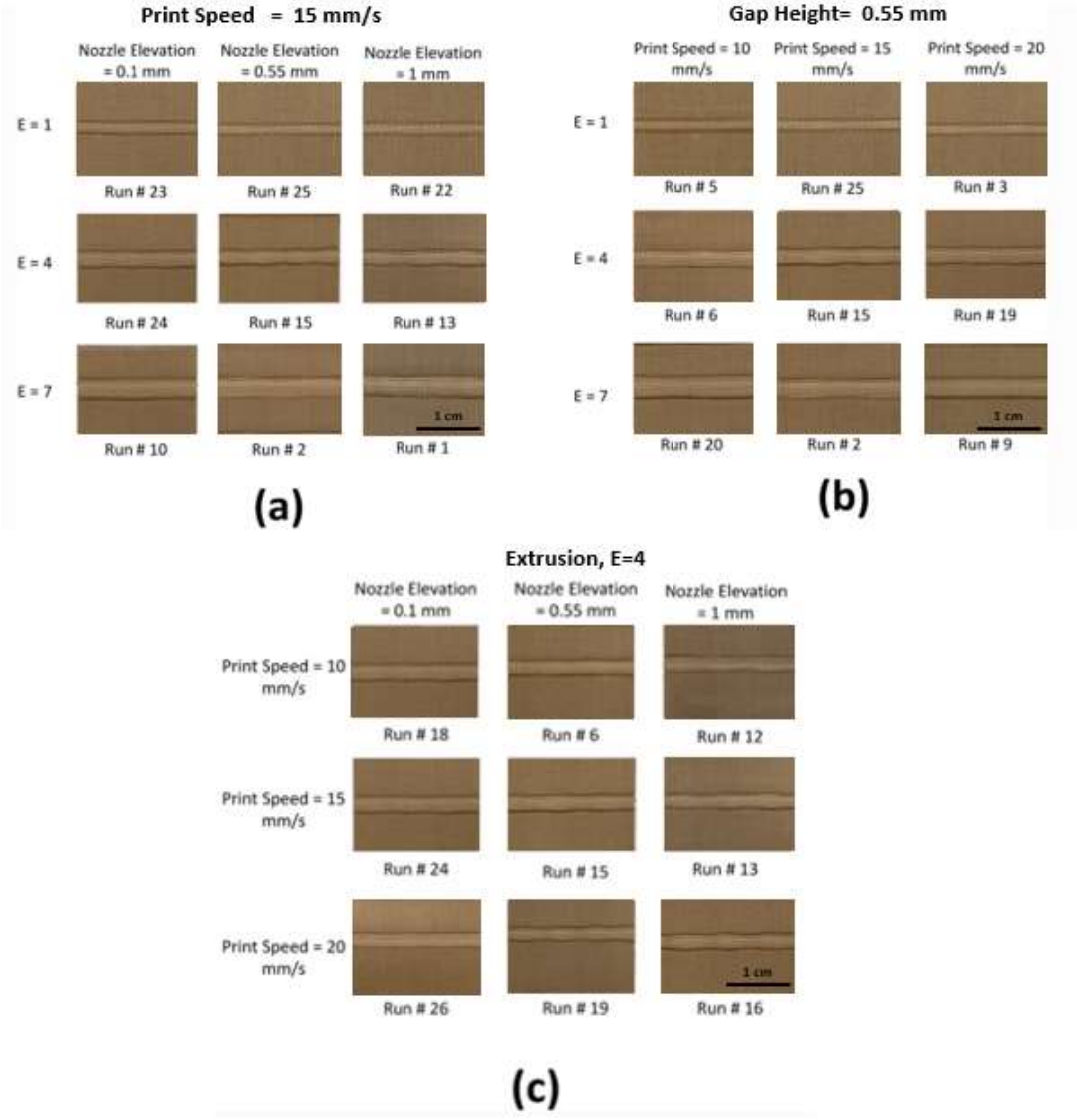

Figure 22: 10 weight percent print width DOE runs.

Figure 23 shows the quantitative line width changes for 10 weight percent EC printed with different parameters. As expected, at a constant extrusion value the line width remains relatively constant. Additionally, when extrusion value is altered, we see large changes in line width, whereas changes due to other parameters seem insignificant. Therefore, extrusion value is the dominant parameter controlling line width.

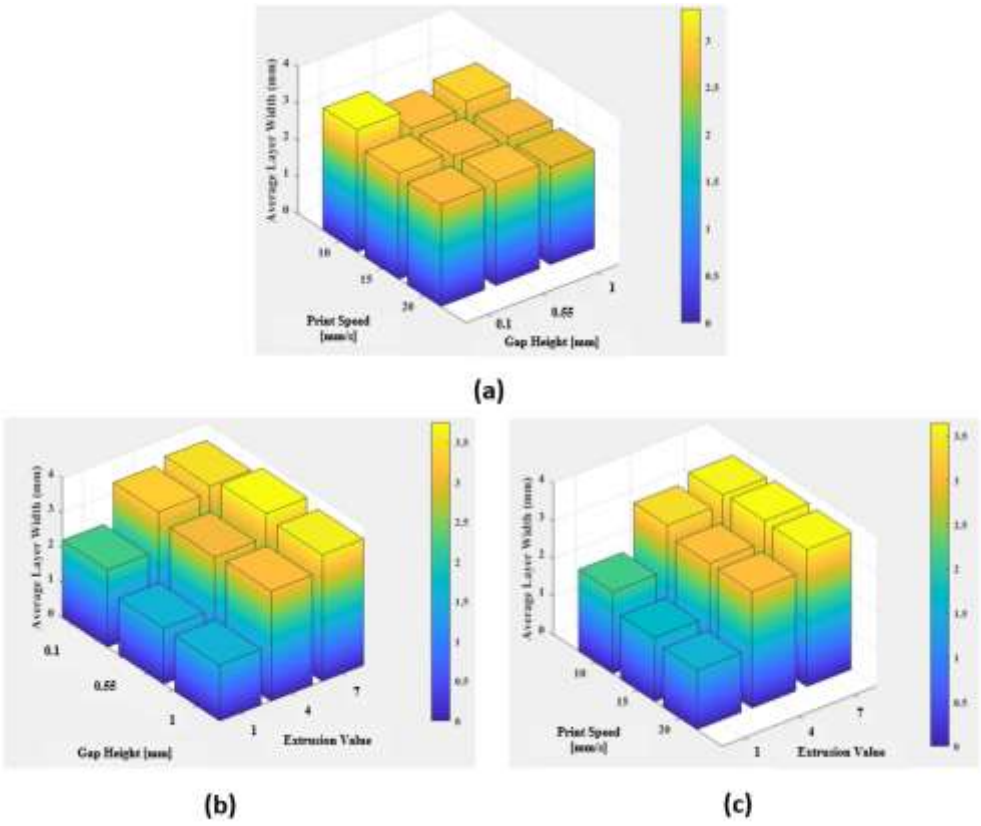

Figure 23: 10 weight percent EC printability DOE parameter plots showing (a) print speed and gap height; (b) gap height and extrusion value; (c) print speed and extrusion value.

While the results show extrusion is the dominant parameter controlling line width, there are some discrepancies regarding the other parameters. At the slowest print speed, we see some higher line widths (Figures 23a, 23c). A similar result can be found in the mass deposition

investigation with an extrusion step of 5. It appears that the linear approximation begins to fail at this edge of the window with further testing. It is not nearly as influential as the extrusion, but is an important interpretation to guide future printing. This result shows that although the uniform deposition at various speeds seemed valid, the only guarantee is to hold print speed constant throughout the reminder of any individual print. An additional observation to be made is that width occasionally increases at lower gap heights (Figure 23b). This result is likely due to slight force or interference with the nozzle during printing.

The 10 weight percent EC results follow previous conclusions by Adams [16] regarding an 8 weight percent EC with similar consistent results. However, Adams concluded that inks greater than 11 weight percent EC were unable to print using the auger screw and 0.6mm nozzle. Despite Adams's claims, higher weight percent inks are required to have effective curing, and thus must be printed.

Figure 24 shows the line width analysis of a 12 weight percent EC ink printed. Overall, similar trends are present, with extrusion value dominating line width trends. However, a larger discrepancy from the expected trends occurs, and print width inconsistencies appear. With higher solid content inks at high extrusion, print width inconsistencies also became apparent (that is, the line would not maintain a smooth edge profile). Instead, it appeared to oscillate without the presence of tunnelling.

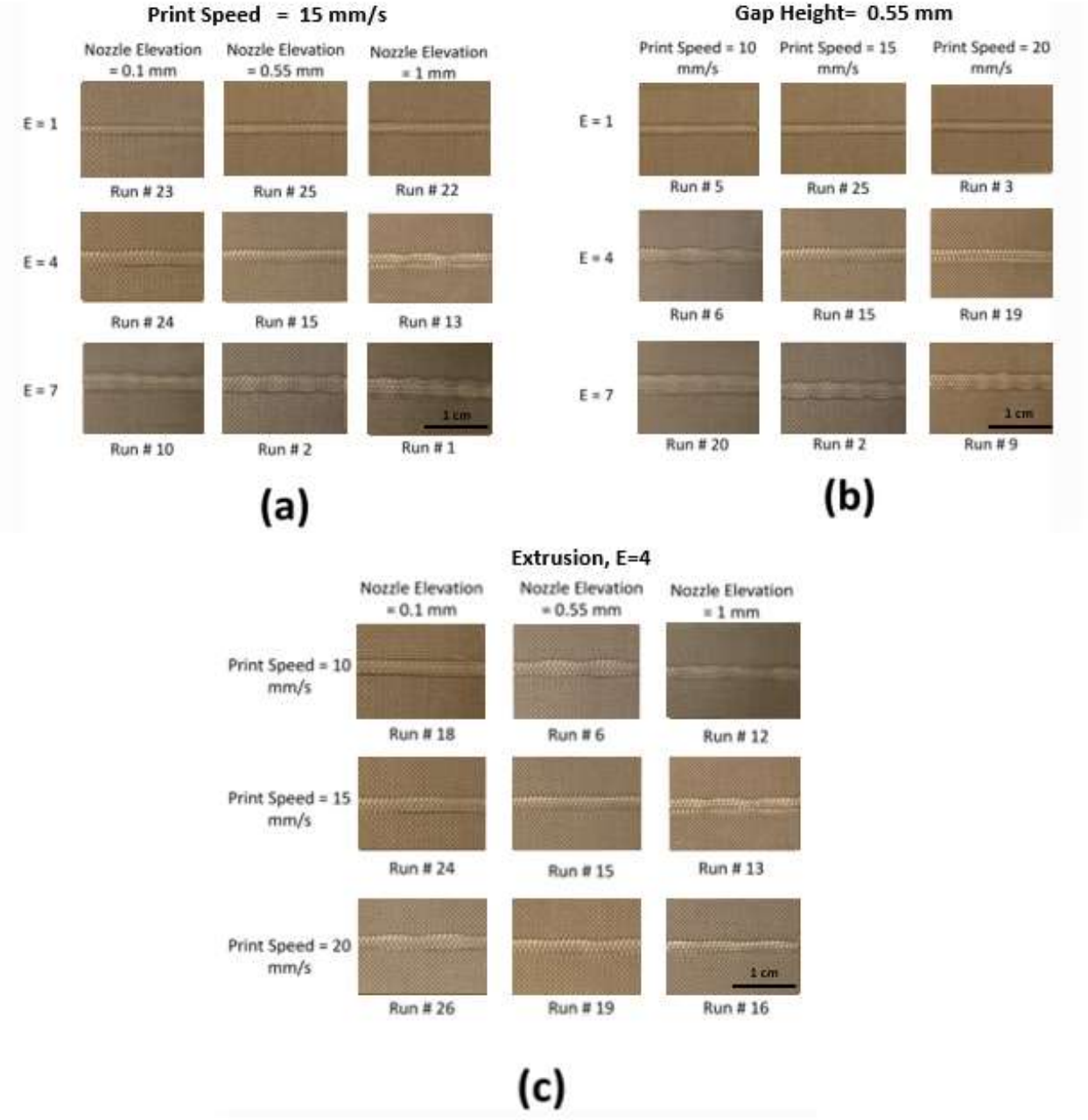

Figure 24:12 weight percent DOE runs.

There is a decrease in repeatability in some cases, but still within reasonable limits. Additionally, the overall max width printed has decreased from roughly 3.5mm to 3mm when compared to 10 weight percent EC ink, see Figure 25. The decrease in print width displays the

direct impact viscosity has on the printing process. Despite the same print parameter operations, the more viscous slurry flows less, yielding a thinner print bead.

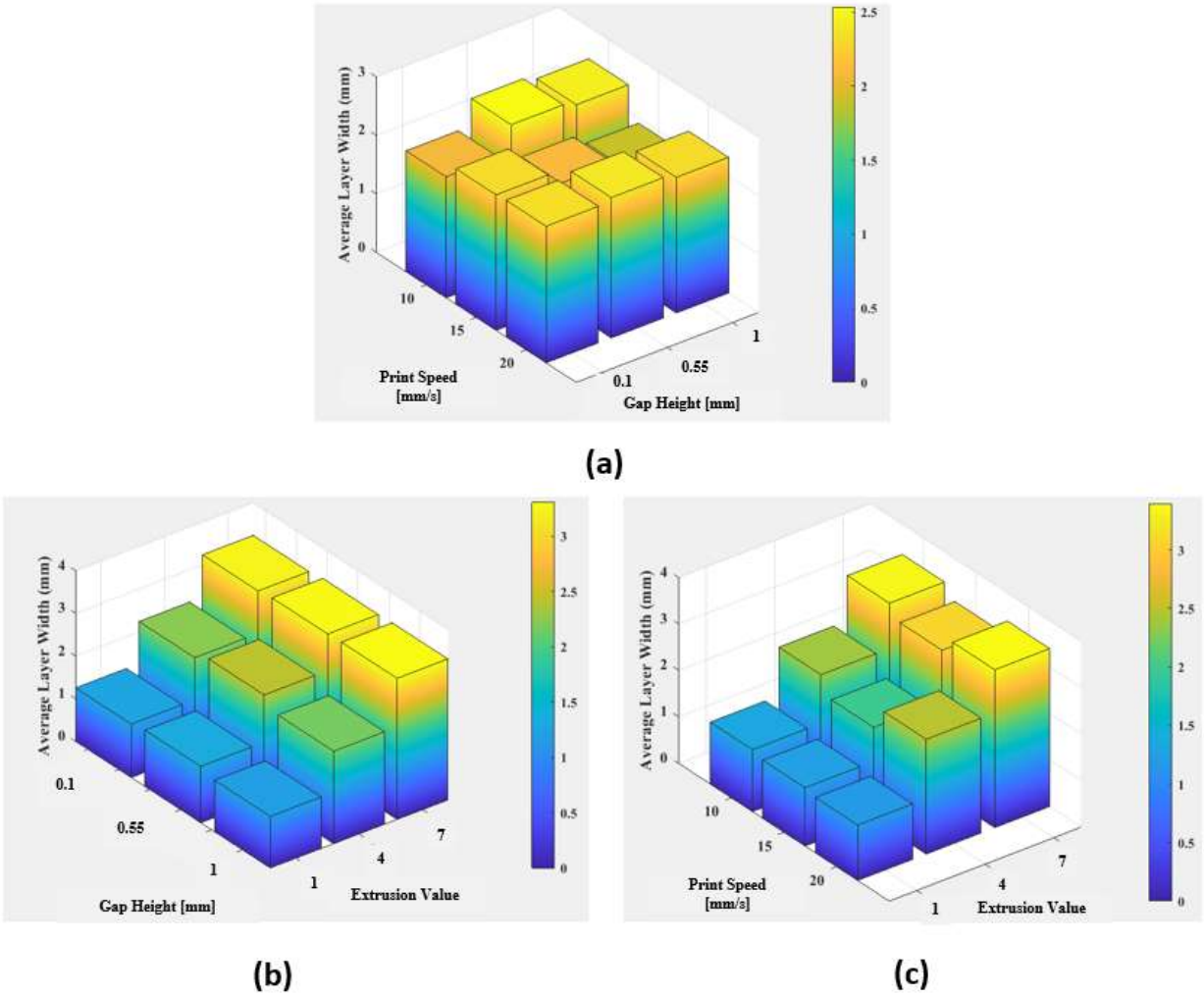

Figure 25: 12 weight percent EC printability DOE parameter plots.

The results indicate a parameter operation window shrinking. At moderate to low print speeds with low extrusion, the ink is printed more consistently and following expected trends. A moderate to large extrusion yields more unpredictability, and unexpected results with the 12 weight percent EC ink. Although the printer is capable of printing over the entire parameter range, the quality of the print window is shrinking.

Figure 26 are the prints for the 15 weight percent EC ink.

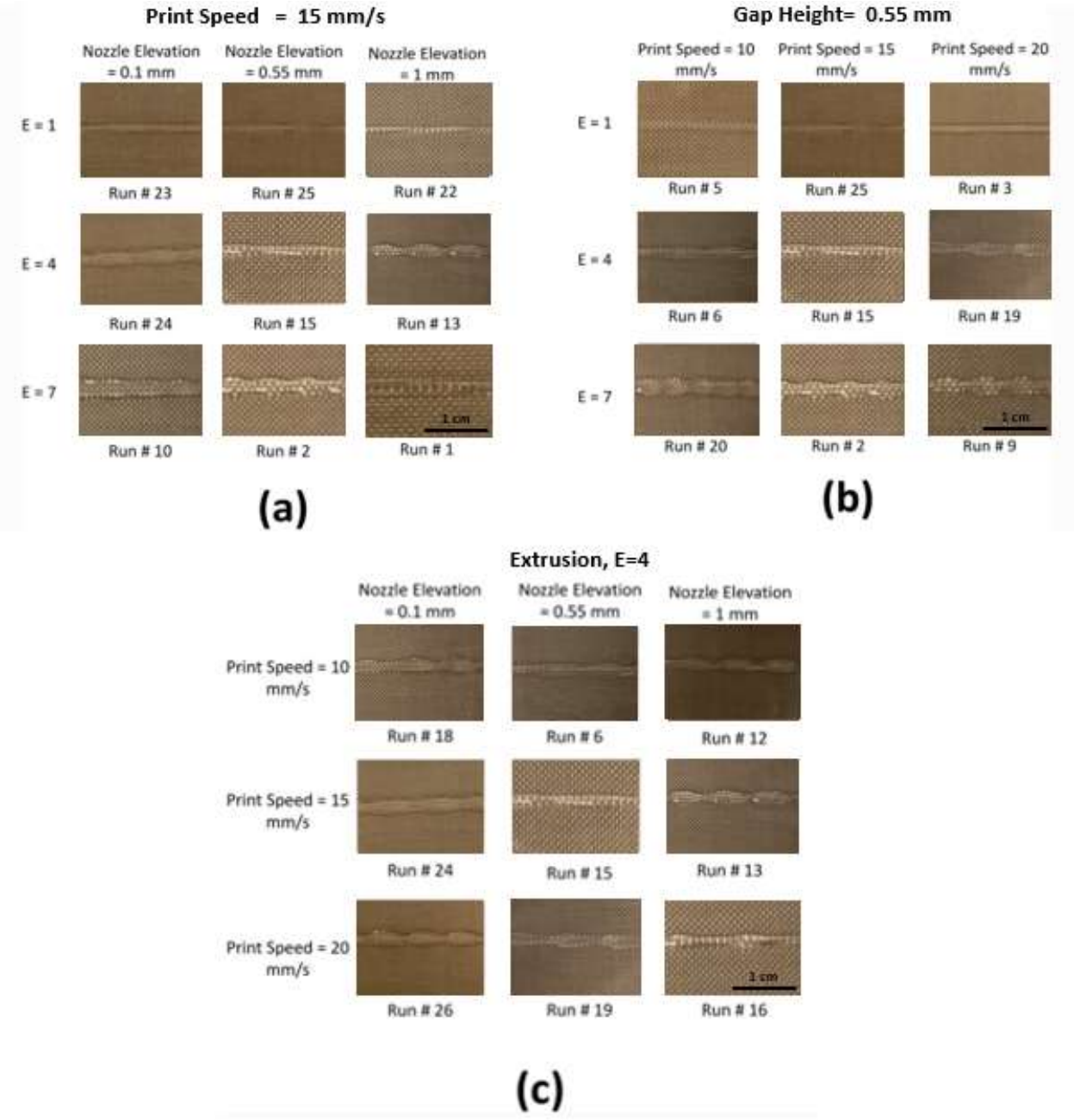

Figure 26: 15 weight percent printed lines.

Figure 27 shows the printability width assessment of 15 weight percent EC ink. The previous trends become more difficult to observe to the point where some results appear random.

As the viscosity increases at higher weight percents, the irregularities become more apparent and smooth profiles can only be seen at low extrusion. Like 12 weight percent EC ink, at low extrusion values the ink prints as expected (Figures 27b and 27c), with print speed and gap height having no significant impact on print results. Despite large variation and unpredictability in trends with high weight percent printing, a subset of parameters seems to maintain expected results. This result suggests that accurate high weight percent EC ink printing can be accomplished, but only using a more restrictive subset of operating conditions.

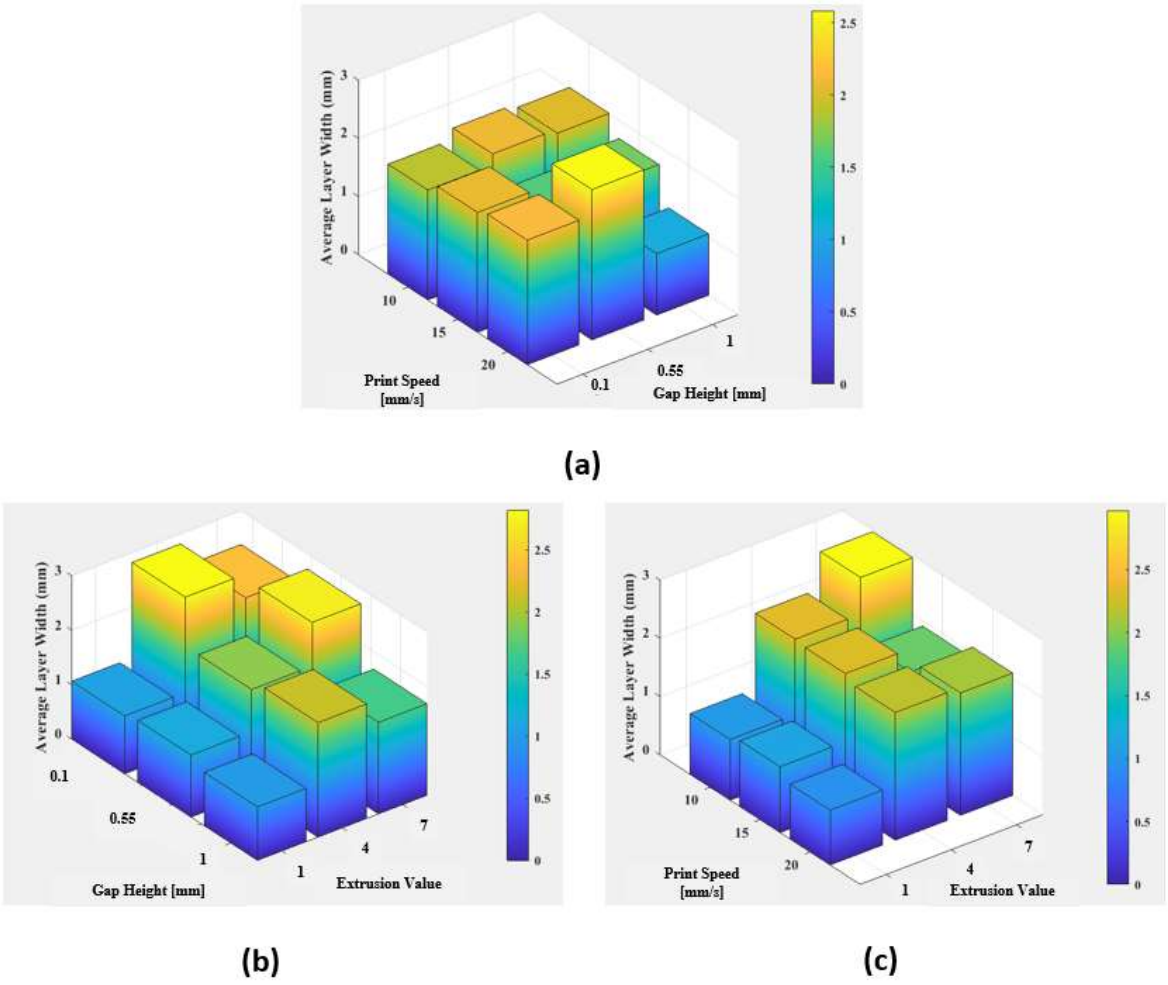

Figure 27: 15 weight percent EC printability DOE parameter plots.

3.2 Impact of EC loading on Curing Behavior

This section of the thesis reviews the results found investigating the curing of printed inks using an IR lamp. With the capability of printing 15 weight percent pure EC, which shows limited spread post print, this ink was selected to attempt curing. Lines were printed with extrusion step of 4, length of 100mm, and cured with the IR lamp at 100 degrees Celsius. Despite the increase in viscosity, the spread during curing is substantial, see Figure 28.

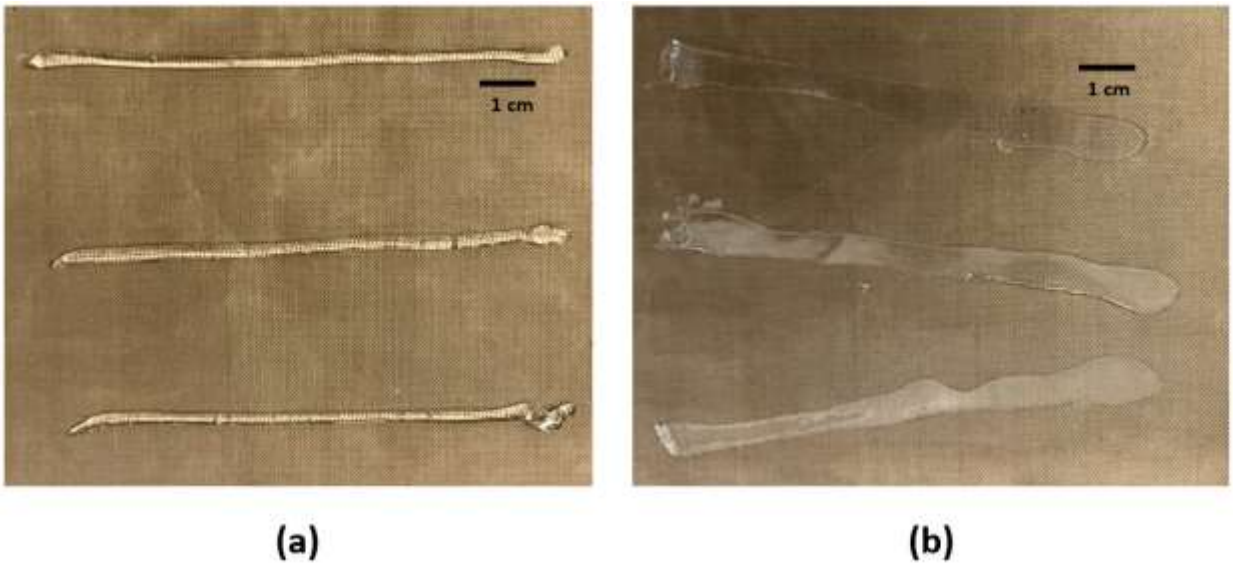

Figure 28: 15 weight percent EC printed with extrusion step of 4 at 100mm cured via IR lamp at 100 degrees C where (a) is before curing and (b) is after curing.

The extreme spreading can be seen in Figures 28a and 28b. Using ImageJ, the measured average spread percentage for these lines ranges around 125-150%. Spreading limits resolution capabilities and enhances inaccuracy or print failure. To achieve higher print quality, spreading must be addressed.

However, depending on the application of the printer, spreading may be advantageous to develop quality prints. Films perform better as a continuous profile, where individual print lines

create surface roughness and reduced mechanical strength. The spreading creates a unform profile with consistent print heights. An example of this potential can be seen in Figure 29, where 13 weight percent EC ink was printed in 2 × 3 cm rectangles. The film thickness is denoted in the image. However, this application is very specific and limits the capabilities of layering.

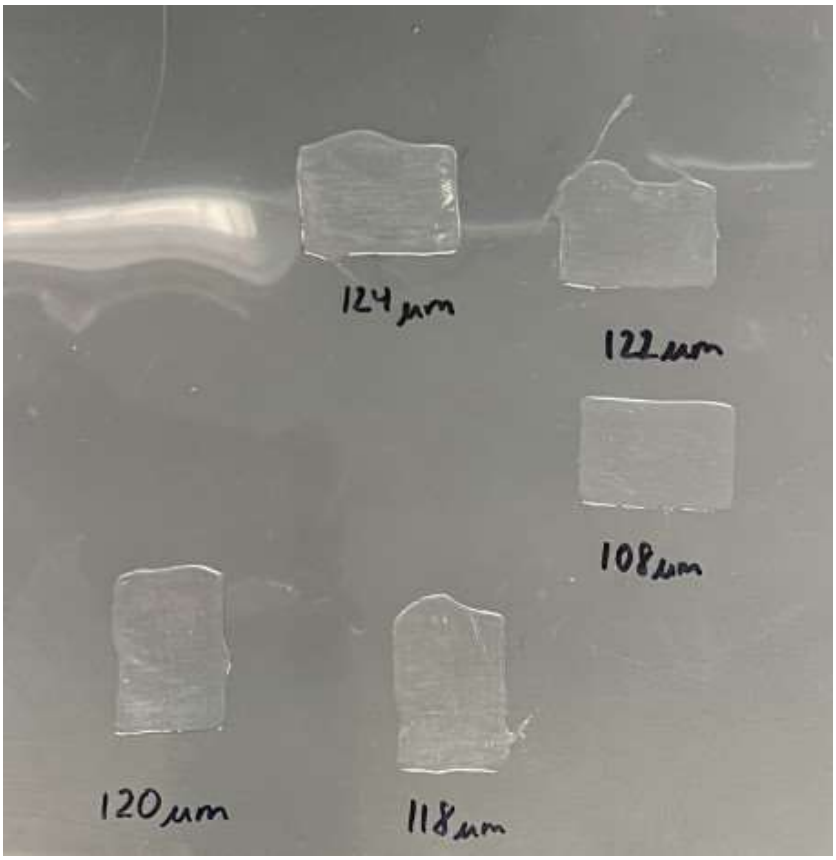

Figure 29: 13 weight percent EC ink printed into 2 x 3 cm film rectangles.

3.3 Impact of Silica on Curing Behavior

With the addition of silica to the slurry, the ink became extremely viscous, but cohesive. A series of slurries were created to see what ranges of EC with silica displayed the shift in properties, and which ones were the best. A range of slurries were created with the intention of raising the EC

weight percent while maintaining printability. The ink range was chosen at the higher end of previous pure EC solute ink printing capabilities (Table 3).

Table 3: Silica loaded composition properties.

Total Solute wt%	EC wt%	Silica wt%	Ratio (EC:Silica)	Property Present
21	18	3	6	yes
19.5	17	2.5	6.8	yes
17.5	15	2.5	6	yes
17.5	12.5	5	2.5	no
14	12	2	6	no

From the small number of samples developed, the cohesive property shift appeared to occur with any slurry above 15 weight percent EC and above 2.5 weight percent silica. Regarding qualitative observations, the 17 weight percent EC with 2.5 weight percent silica had the most consistency. The other compositions seemed operational. The lower weight percents started to lack the cohesive nature, while the higher were difficult to create and somewhat clumpy.

During preliminary trials the ink had no visible spreading post cure and had strong structural integrity. Although it could print, the purpose of adding silica was to provide structural support during the curing process. Initial testing shows a significant decrease in spreading, see Figure 30.

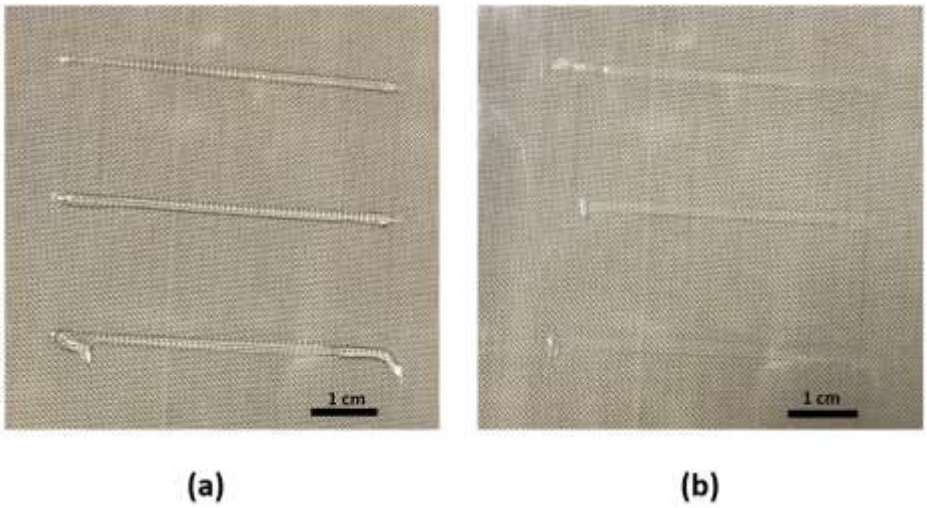

Figure 30: 17 weight percent EC with 2.5 weight percent silica ink printed with extrusion step of 1 at 50mm cured via IR lamp at 100 degrees C with (a) prior to the cure and (b) post cure.

The addition of silica in combination with raising the total solute content led to a reduction in spread percentage during the curing process. For a more thorough understanding, the developed inks were printed and then cured at various temperatures (Table 4). Figure 31 shows the curing results plotted for each composition.

Table 4: Curing conditions with different compositions at different temperatures.

Ethyl Cellulose [weight %]	Silica [weight %]	Temperature Goal [Degrees Celsius]	Z-Axis position Estimation [mm]	Time to Cure [min:second]	Spread Percentage
18	3	110	220	6:14	38.68
18	3	130	180	5:40	12.97
18	3	150	130	3:45	34.34
17	2.5	110	220	6:07	14.51
17	2.5	130	180	4:50	8.67
17	2.5	150	130	3:30	14.64
15	2.5	110	220	6:00	48.39
15	2.5	130	180	5:00	18.54
15	2.5	150	130	3:30	27.18

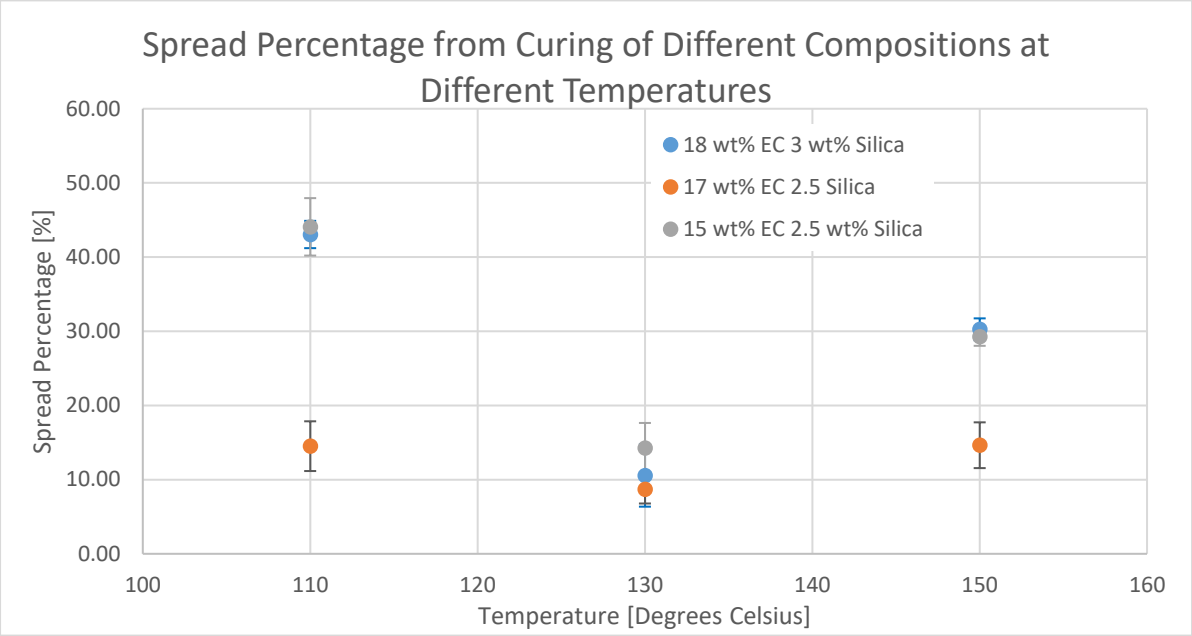

Figure 31: Spread percentage of various slurry compositions at various temperatures using the infrared radiation lamp.

All slurry compositions showed a major reduction in spread percentage when cured, with 17 weight percent EC and 2.5 weight percent silica never above 15% spread. Qualitatively, this ink printed higher quality lines with more ease as opposed to the other slurries as well. Additionally curing at 130^{o}C appears to reduce spread for all ink compositions.

To understand and quantify the curing results, the glass transition temperature was extracted through DSC analysis for each cured composition at each temperature (Table 5). A higher glass transition temperature typically indicates a better quality of cure.

Table 5: DSC Glass Transition Temperature

Composition [EC wt%]	Composition [Silica wt%]	Temperature [Degrees Celsius]	Weight [grams]	Glass Transition Temp [Degrees Celsius]	Average	Standard Deviation
18	3	110	4.4	119	118	1.020
			4.1	117		
			4.4	118		
		130	4	117	111	5.718
			4.2	109		
			4.2	107		
		150	4	118	115	4.043
			4.2	116		
			4.1	110		
17	2.5	110	4.1	117	115	2.044
			4.2	115		
			3.9	113		
		130	3.8	119	116	2.985
			4.3	116		
			4.2	113		
		150	4.2	111	115	3.786
			4.3	118		
			3.7	117		
15	2.5	110	3.8	114	114	2.517
			3.9	117		
			3.9	112		
		130	4.3	107	107	0.000
			4.3	107		
			4	107		
		150	4.2	111	115	3.786
			4.1	118		
			4.1	117		

To visualize this data, a plot was created with error bars representing a single standard deviation in each direction (Figure 32).

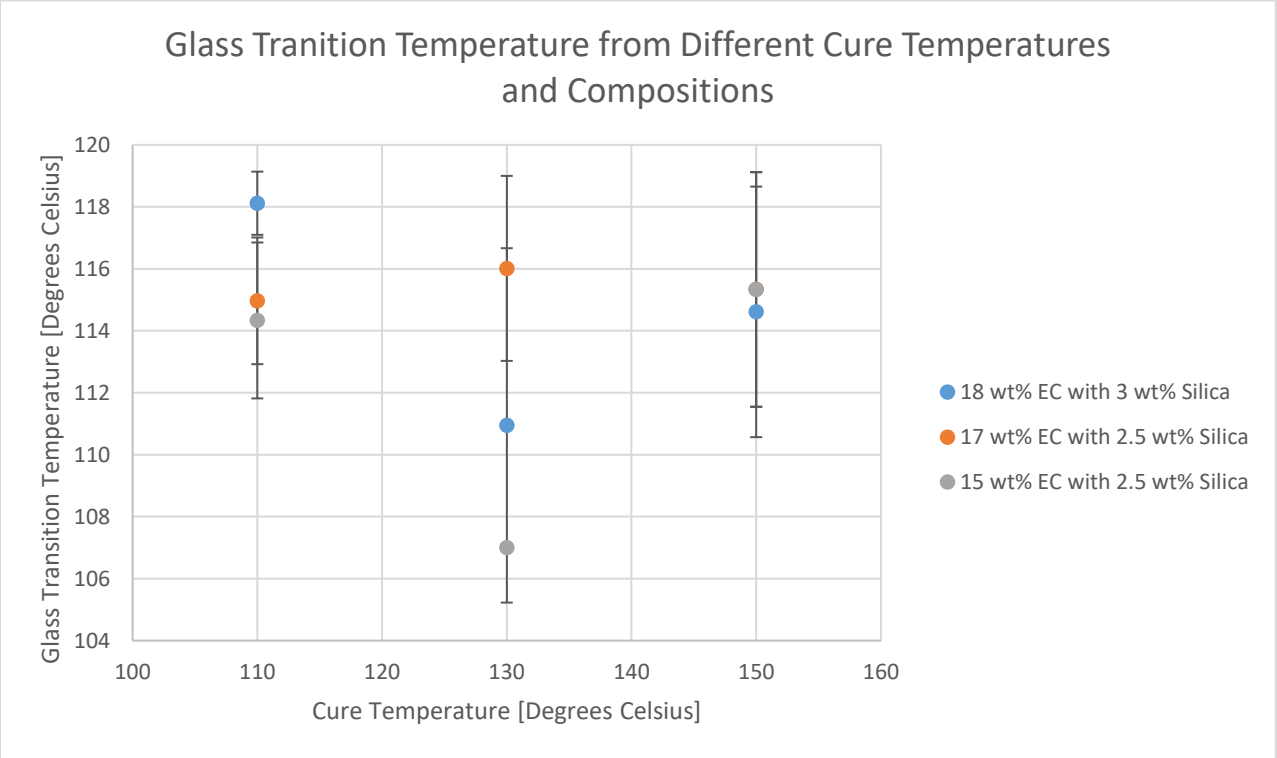

Figure 32: Glass Transition Temperature from Different Cure Temperatures and Compositions.

There is no statistically significant difference between the glass transition temperatures of each composition, so they are thermally similar. Therefore, no differences in thermal properties are expected between various inks.

In addition to the glass transition temperature, the differences between the first and second heat reveal information about the composition of the cured ink. The first heat burns any remaining solvent and impurities. Upon running DSC on the cured samples, a consistent peak was observed around 150-220 ^{o}C (Figure 33).

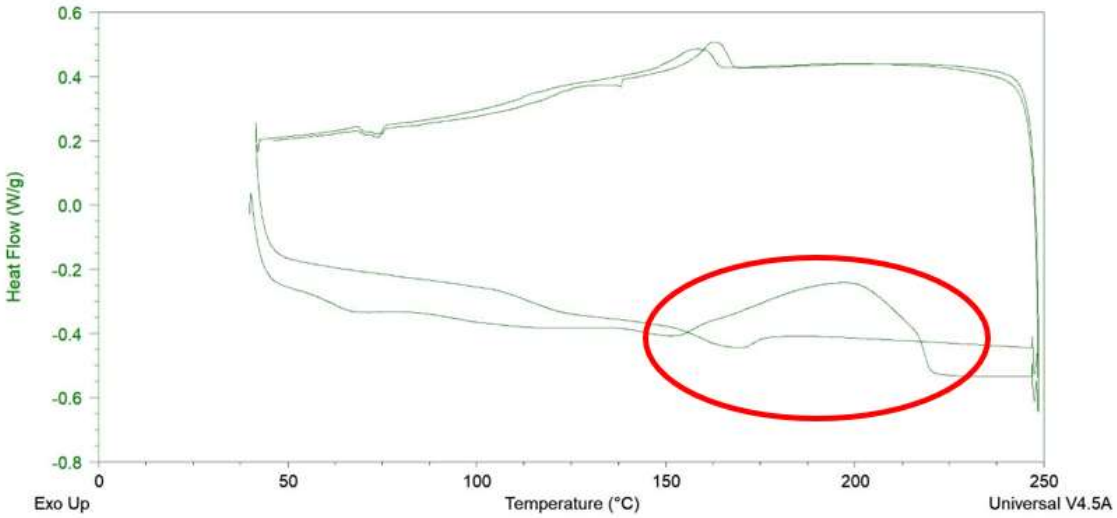

Figure 33: 17 weight percent EC with 2.5 weight percent Silica DSC solvent peak.

This peak corresponds to the findings of Li et al, who ran DSC testing on a zinc-based paste with alpha terpineol as the solvent [28]. Their results concluded most of weight loss during testing is attributed to the removal of terpineol, which can be visualized by a peak in the DSC first heat from 120-180 ^{o}C [28]. Therefore, it was ascertained that the peak in the first heat observed is removal of the solvent alpha terpineol. When comparing the solvent peak, there were differences in peak height relative to curing temperature (Figure 34).

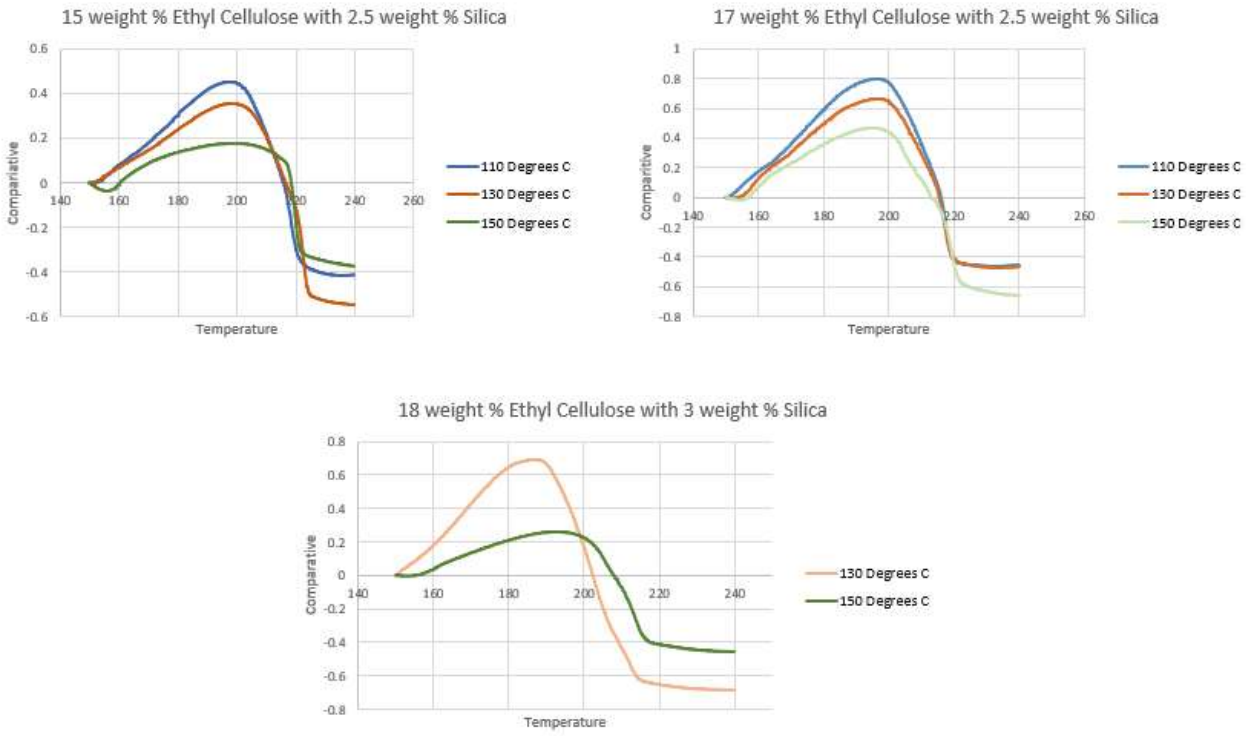

Figure 34: First heat solvent removal peak for each composition at various cure temperatures.

For each cure temperature, a representative curve was selected for each set of samples tested. Due to a procedural change in ramp rate during testing, the 18 weight percent EC and 3 weight percent silica at 110 ^{o}C cure temp were not included to maintain the validity of the comparison. The solvent peak flattens as the cure temperature rises in each composition. From this result, it can be concluded that the increase in cure temperature removed more solvent during the curing process. Therefore, the higher cure temperature up to 150^{o}C yields a cured print containing less solvent.

Chapter 4

Analysis and Conclusions

4.1 Ethyl Cellulose Printability

The printability study first required an analysis of the printing parameters, gap height, print speed, and extrusion. Gap height and print speed were unchanged from the original printer operations. However, the extrusion parameter has been manipulated from a feeding mechanism to driving a stepper motor for extrusion. Through testing, the extrusion parameter was found to control the number of revolutions, with 1 equating to 1.81 revolutions.

By testing post print spread of EC inks ranging from 5-15 weight percent, an inverse relationship was observed between weight percent and spreading. Higher solid content yielded less spreading and more continuity. Therefore, the goal was to determine viable printing parameters to print higher solid contents.

Preliminary trials using a 0.6mm nozzle and 10 weight percent EC ink indicated a viable print window for each value with print speed ranging from 10-20 mm/s, gap height ranging from 0.1-1mm, and extrusion ranging from 1-7. As expected, print speed and gap height have minimal effect, while extrusion dominates print width. When the solid content is increased, deviation from the expected trend is amplified. Despite high solid content, with low extrusion the trends are maintained. Although it was previously determined that EC inks above 11 weight percent solid content are unprintable with the system, the results show a reduced viable printing window, namely extrusion. At higher weight percent inks, the printer operates well with an extrusion value of 1,

gap height at or below 0.55, and a print speed of 15-20. This range is tested and validated for EC inks up to 15 weight percent.

4.2 Curing

Upon printing, the material must be cured to get rid of the solvent and solidify the resulting print. The curing process must occur within a realistic time frame and feasible to incorporate with the printer. It is found that a mounted IR lamp provides relatively quick curing times with minimal intrusion or shifting of the printed material. Pure EC inks experience extreme spreading during curing, with spreading exceeding 200 percent of the original width. Therefore, additives, namely silica, were added to provide structural integrity throughout the curing process. With the addition of silica, a shift in property emerged, where the ink became cohesive as opposed to adhesive. This property shift developed an ink without any spread after printing, and a significant reduction in spread during curing. All spread percentages were under 50 percent and in many cases under 20 percent. Although the solid content was increased, the cohesiveness of the resulting material maintained the ability to print at solute contents exceeding 20 weight percent. Additionally, silica reduced cure times from 10-15 minutes to under 7 minutes. Shorter cure times result in less overall manufacturing time.

Of the EC silica inks tested, the 17 weight percent EC with 2.5 weight percent silica consistently spread the least and printed at a higher quality in comparison to other inks. The material viscosity seemed to work well with the system, having the needed internal integrity, but maintaining a smooth flow during extrusion. Of the three tested temperatures, 130 ^{o}C yielded the

lowest spreading for each composition of ink. However, through DSC testing, it was found that a 150^{o}C cure temperature yields a print with the least amount of solvent remaining. Depending on the application of the print and the desired behavior, the cure temperature could be used as a tool to manipulate properties.

4.3 Future Research and Development

Future developments from this research could take three main directions: optimizing printing for layered complex geometries using the EC-Silica ink, improving the mechanical design, and testing other materials or EC composites.

This research did not investigate layering but provided a foundation to continue the analysis in this direction. Layering is effectively an extension of the curing process. Physically printing layers is not a challenge, but understanding the relationships between each layer through curing is unknown. Proper curing percentage between each layer ensures layer adhesion while maintaining layer integrity. The largest challenge relates to layer overlap restraints. On traditional PLA printers, layers can print with only 50% overlap, yielding a potential for 45-degree angles without the requirement of support structures. Current testing only considered 100 percent overlap between layers. Although it seems unlikely for this method of printing to achieve a reduced layer overlap, it is a challenge to be investigated. The curing process also has much room for further research. Quantitatively there are many more material tests that could be used, as well as alternative curing processes.

Although the mechanical design functions well for a prototype, improvements to the printer itself could increase print quality and improve the resolution. The selected nozzles (0.6mm and 1mm) could be altered to best fit a given application. Additionally, the 3D printed printhead casing could be fabricated to improve surface finish and reduce risk of deformation and clogging. A major area of mechanical design improvements would be the curing system. In the current setup the IR lamp must be placed and then removed for each layer. Therefore, a multilayer print requires manual interaction after each printed layer to begin curing. The entire print process could theoretically be automated, where after the print the print bed dropped to a certain height to cure, and the curing lamp would turn on for a set time. For this to be accomplished a new mount would have to be developed and a power switch output from the printer to the lamp.

The final and most versatile area of future work would be printing other materials or introducing other EC composites. The current printer setup has provided proof of concept of custom DIW of biopolymer inks, but it is not exclusive to EC or EC with silica. Within the lifetime of the printer other researchers have also successfully printed BTO composites. Other materials and other EC composites have the potential to be printed but need printability maps built to discover the operating print parameters.

BIBLIOGRAPHY

[1] S. Wasti and S. Adhikari, "Use of Biomaterials for 3D Printing by Fused Deposition Modeling Technique: A Review," *Frontiers in Chemistry*, vol. 8, p. 315, May 2020, doi: 10.3389/FCHEM.2020.00315/BIBTEX.

[2] C. S. Wu and H. T. Liao, "Fabrication, characterization, and application of polyester/wood flour composites," *Journal of Polymer Engineering*, vol. 37, no. 7, pp. 689–698, Sep. 2017, doi: 10.1515/POLYENG-2016-0284/MACHINEREADABLECITATION/RIS.

[3] M. Davidovich-Pinhas, S. Barbut, and A. G. Marangoni, "Physical structure and thermal behavior of ethylcellulose," *Cellulose*, vol. 21, no. 5, pp. 3243–3255, 2014, doi: 10.1007/S10570-014-0377-1.

[4] "Dr. L. Lilienfeld," *Nature 1938 142:3589*, vol. 142, no. 3589, pp. 282–282, Aug. 1938, doi: 10.1038/142282b0.

[5] Q. Wang, J. Sun, Q. Yao, C. Ji, J. Liu, and Q. Zhu, "3D printing with cellulose materials," *Cellulose 2018 25:8*, vol. 25, no. 8, pp. 4275–4301, Jun. 2018, doi: 10.1007/S10570-018-1888-Y.

[6] H. C. Haas, L. Farney, and C. Valle, "Some properties of ethyl cellulose films," *Journal of Colloid Science*, vol. 7, no. 6, pp. 584–599, Dec. 1952, doi: 10.1016/0095-8522(52)90041-X.

[7] P. W. S. Heng, L. W. Chan, and K. T. Chow, "Development of Novel Nonaqueous Ethylcellulose Gel Matrices: Rheological and Mechanical Characterization," *Pharmaceutical Research 2005 22:4*, vol. 22, no. 4, pp. 676–684, Apr. 2005, doi: 10.1007/S11095-005-2484-Z.

[8] P. Ahmadi, A. Jahanban-Esfahlan, A. Ahmadi, M. Tabibiazar, and M. Mohammadifar, "Development of Ethyl Cellulose-based Formulations: A Perspective on the Novel Technical Methods," *https://doi.org/10.1080/87559129.2020.1741007*, 2020, doi: 10.1080/87559129.2020.1741007.

[9] N. Paxton, W. Smolan, T. Böck, F. Melchels, J. Groll, and T. Jungst, "Proposal to assess printability of bioinks for extrusion-based bioprinting and evaluation of rheological properties governing bioprintability," *Biofabrication*, vol. 9, no. 4, Nov. 2017, doi: 10.1088/1758-5090/AA8DD8.

[10] L. W. McKeen, "Renewable Resource and Biodegradable Polymers," *Film Properties of Plastics and Elastomers*, pp. 353–378, Jan. 2012, doi: 10.1016/B978-1-4557-2551-9.00014-1.

[11] L. H. P. Jones and K. A. Handreck, "Silica In Soils, Plants, and Animals," *Advances in Agronomy*, vol. 19, no. C, pp. 107–149, Jan. 1967, doi: 10.1016/S0065-2113(08)60734-8.

[12] T. Wohlers and T. Gornet, "History of Additive Manufacturing," 2014.

[13] I. Karakurt and L. Lin, "3D printing technologies: techniques, materials, and post-processing," *Current Opinion in Chemical Engineering*, vol. 28, pp. 134–143, Jun. 2020, doi: 10.1016/J.COCHE.2020.04.001.

[14] M. Schmid, A. Amado, and K. Wegener, "Materials perspective of polymers for additive manufacturing with selective laser sintering," *Journal of Materials Research*, vol. 29, no. 17, pp. 1824–1832, Jun. 2014, doi: 10.1557/JMR.2014.138.

[15] F. Fina *et al.*, "3D printing of drug-loaded gyroid lattices using selective laser sintering," *International Journal of Pharmaceutics*, vol. 547, no. 1–2, pp. 44–52, Aug. 2018, doi: 10.1016/J.IJPHARM.2018.05.044.

[16] D. Adams, Z. Ounaies, and A. Basak, "Printability Assessment of Ethyl Cellulose Biopolymer Using Direct Ink Writing," *JOM*, vol. 73, no. 12, pp. 3761–3770, Dec. 2021, doi: 10.1007/S11837-021-04911-8/TABLES/2.

[17] S. Wickramasinghe, T. Do, and P. Tran, "polymers FDM-Based 3D Printing of Polymer and Associated Composite: A Review on Mechanical Properties, Defects and Treatments," 2020, doi: 10.3390/polym12071529.

[18] Y. Yang, H. Wang, H. Li, Z. Ou, and G. Yang, “3D printed tablets with internal scaffold structure using ethyl cellulose to achieve sustained ibuprofen release,” *European Journal of Pharmaceutical Sciences*, vol. 115, pp. 11–18, Mar. 2018, doi: 10.1016/J.EJPS.2018.01.005.

[19] P. Menčík *et al.*, “Effect of Selected Commercial Plasticizers on Mechanical, Thermal, and Morphological Properties of Poly(3-hydroxybutyrate)/Poly(lactic acid)/Plasticizer Biodegradable Blends for Three-Dimensional (3D) Print,” *Materials 2018, Vol. 11, Page 1893*, vol. 11, no. 10, p.1893, Oct. 2018, doi: 10.3390/MA11101893.

[20] V. C. F. Li, C. K. Dunn, Z. Zhang, Y. Deng, and H. J. Qi, “Direct Ink Write (DIW) 3D Printed Cellulose Nanocrystal Aerogel Structures,” *Scientific Reports 2017 7:1*, vol. 7, no. 1, pp. 1–8, Aug. 2017, doi: 10.1038/s41598-017-07771-y.

[21] S. v. Murphy and A. Atala, “3D bioprinting of tissues and organs,” *Nature Biotechnology*, vol. 32, no. 8, pp. 773–785, 2014, doi: 10.1038/NBT.2958.

[22] L. Johnson *et al.*, “Assessing printability maps in additive manufacturing of metal alloys,” *Acta Materialia*, vol. 176, pp. 199–210, Sep. 2019, doi: 10.1016/J.ACTAMAT.2019.07.005.

[23] Z. A. Hoopes, M. L. Karschner, J. Kelly, W. B. Miney, Z. Ounaies, and A. Basak, “Printability Assessment of Cellulose-Based Polymer Structures using Direct Ink Writing”.

[24] “Download.” https://imagej.nih.gov/ij/download.html (accessed Mar. 31, 2023).

[25] H. Li, Z. Xie, Y. Zhang, and J. Wang, “The effects of ethyl cellulose on PV performance of DSSC made of nanostructured ZnO pastes,” *Thin Solid Films*, vol. 518, no. 24, pp. e68–e71, Oct. 2010, doi: 10.1016/J.TSF.2010.03.125.

[26] A. Shrivastava, “Introduction to Plastics Engineering,” *Introduction to Plastics Engineering*, pp. 1–16, Jan. 2018, doi: 10.1016/B978-0-323-39500-7.00001-0.

[27] M. Dewaele *et al.*, “Influence of curing protocol on selected properties of light-curing polymers: Degree of conversion, volume contraction, elastic modulus, and glass transition temperature,” *Dental Materials*, vol. 25, no. 12, pp. 1576–1584, Dec. 2009, doi:

10.1016/J.DENTAL.2009.08.001.

ACADEMIC VITA

EDUCATION

The Pennsylvania State University *Spring 2023 | University Park, PA*
Schreyer Honors Scholar, B.S. in Mechanical Engineering

EXPERIENCE

Turbine Design Engineering Intern *Summer 2022 | Voith Hydro | York PA*

- Develop professional drafting skills modeling turbine components for manufacturing with SolidEdge
- Design manufacturing and installation devices using ANSYS FEA analysis to verify standard FOS
- Demonstrate ability to adapt and iterate models/drawings to align with feedback from design reviews

Engineering Intern *Summer 2021| UTZ LLC | Hanover PA*

- Draft production models with integrated machine design to increase and expand production efficiency
- Act as assistant project manager to install new kettle and packaging line, expanding production 15%

Maker Space Assistant *Fall 2020-Spring 2021 | Penn State University*

- Polish speaking skills by lecturing SolidWorks and drafting techniques to 30 students 6 hours weekly

INVOLVMENT

Biopolymer 3D Printing Undergraduate Research *Fall 2021-Present | Penn State University*

- Printability assessment of Ethyl Cellulose using direct ink writing for additive manufacturing
- Work 10-15 hours in the lab per week performing experimental trials and data analytics for thesis
- Practice professional leadership skills training new lab members in lab operations and safety

Fall League Director Club Baseball *Fall 2019 - Present | Penn State Club Baseball*

- Organize recreational league and professional showcase for 150 prospects of the club baseball team
- Develop time management and teamwork skills competing with a team of 50 students-athletes

PROJECTS

NYPA Jack Screw Testing Device Design *Summer 2022 |Voith Hydro*

- Designed a device allowing simultaneous strain gauge testing on 12 thrust bearing jack screws withstanding 25 ton per screw

- Optimized design by eliminating excess hydraulic rams, saving at least 55 thousand in equipment cost while also minimizing material cost

Maintenance Floorplan Redesign *Summer 2021 |UTZ Quality Foods*

- Draft floorplan model of existing machining, equipment, etc. for 300x300 ft maintenance space
- Pitch draft designs to maintenance department executives in design reviews
- Contact vendors and outline project timeline and financial plan

Leonard Center Technical Speaking Contest *Spring 2021 |Penn State University*

- Practice professional technical speaking, presenting technical developments in additive manufacturing to an academic panel in speaking contest
- Earned People's Choice Award

SOFTWARE SKILLS

- SolidWorks, Inventor, AutoCAD, MATLAB, ANSYS, Excel, SolidEdge, MathCAD, C, SAP